The Role of MicroRNA-200b in Pulmonary Hypoplasia Associated with Congenital Diaphragmatic Hernia

by

Ramin Kholdebarin

A Thesis submitted to the Faculty of Graduate Studies of

The University of Manitoba

in partial fulfillment of the requirements of the degree of

MASTER OF SCIENCE

Department of Surgery

University of Manitoba

Winnipeg

ABSTRACT

Congenital diaphragmatic hernia (CDH) is a developmental defect of the diaphragm that is associated with pulmonary hypoplasia. The pathophysiology of abnormal lung development in CDH is unknown. MicroRNAs (miRNAs) are small RNA molecules that regulate gene expression through post-transcriptional silencing. A previous microarray screen in pulmonary tissue from human fetuses with CDH found a 50-fold increase in expression of microRNA-200b (miR-200b). In this project we used in situ hybridization to detect miR-200b expression in lungs from human postnatal cases and an animal model of CDH. In human lungs, CDH was associated with increased miR-200b expression. This was most evident in the terminal saccules and alveoli. In rat lungs, nitrofen-induced CDH resulted in decreased pulmonary expression of miR-200b. In early lung development, miR-200b expression was highest in the undifferentiated splanchnic mesenchyme and in distal parabronchial tissue. Its levels dropped in the more proximal parabronchial cells and with increasing gestational age. In pulmonary epithelium, miR-200b expression was highest at the elongating tips of the bronchial tree. Using immunohistochemistry, we detected expression of vimentin, a mesenchymal marker, in the distal epithelium during branching morphogenesis. Based on these observations, we propose a model in which miR-200b contributes to lung development by balancing epithelial proliferation and differentiation through modulation of TGF-β signaling. This model accounts for the observed differences between human and nitrofen-induced CDH.

ACKNOWLEDGEMENTS

The completion of this work would not have been possible without the contribution and support of several individuals.

First and foremost, to my advisor Dr. Richard Keijzer – thank you for giving me the opportunity to be involved in a fascinating research project. I am indebted to you for your guidance and encouragement. Your drive and determination have been a source of inspiration.

To Barbara Iwasiow – your experience and resourcefulness have been invaluable in improving my work. Your energy and enthusiasm are greatly appreciated.

To Naghmeh Khoshgoo – your findings were crucial to the interpretation of my results. Thank you for your assistance in reviewing my thesis.

To Danzhu Mowat and the Department of Pathology – completion of this project would not have been possible without access to your digital microscopy facility.

To Dr. Andrew Halayko, Jacquie Schwartz and Behzad Yeganeh – for all of your advice and expertise.

To my fiancé, April, and my family, thank you for all your love and support throughout this endeavor.

Last but not least, I must acknowledge the generous contribution of various funding agencies including the Manitoba Medical Services Foundation, the Manitoba Institute of Child Health, the Thorlakson Foundation, the Molly Towel Perinatal Research Foundation and a grant from the Clinical Earnings of Academic Surgeons (GFT group, Department of Surgery).

TABLE OF CONTENTS

LIST OF TABLES

LIST OF FIGURES

ABBREVIATIONS

3' UTR	3' untranslated region
AGO	argonaute
AP	alkaline phosphatase
BMP	bone morphogenetic protein
CC-10	clara cell secretory protein-10
CDH	congenital diaphragmatic hernia
CFTR	cystic fibrosis transmembrane conductance regulator
DIG	digoxigenin
E	embryonic day
ECM	extracellular matrix
ECMO	extracorporeal membrane oxygenation
EMT	epithelial-to-mesenchymal transition
FETO	fetal endoscopic tracheal occlusion
FGF	fibroblast growth factor
HFOV	high frequency oscillatory ventilation
HRP	horseradish peroxidase
IHC	immunohistochemistry
iNO	inhaled nitric oxide
IPF	idiopathic pulmonary fibrosis
ISH	in situ hybridization
LNA	locked nucleic acid

MDCK	Madin Darby canine kidney
MET	mesenchymal-to-epithelial transition
miRNA	microRNA
MRI	magnetic resonance imaging
mRNA	messenger RNA
NOG	noggin
PBS	phosphate buffered saline
PFA	paraformaldehyde
PH	pulmonary hypoplasia
PPF	pleuro-peritoneal fold
PPHN	persistent pulmonary hypertension
pre-miRNA	precursor miRNA
pri-miRNA	primary miRNA
PTC	patched
RISC	RNA-induced silencing complex
qPCR	real-time quantitative polymerase chain reaction
SHH	sonic hedgehog
snRNA	small nuclear RNA
SP-A	surfactant protein A
SP-C	surfactant protein C
SPRY	sprouty
SSC	sodium chloride/sodium citrate
TGF-β	transforming growth factor beta

TTF-1	thyroid transcription factor-1
TβR	TGF-β receptor
α-SMA	α-smooth muscle actin

CHAPTER 1. INTRODUCTION

1.1. Epidemiology and Current Treatment

Congenital diaphragmatic hernia (CDH) is a developmental defect of the diaphragm that allows herniation of abdominal viscera into the chest cavity. It occurs with an incidence of 1 in 2000 to 3000 live births[1, 2]. Although the diaphragmatic defect can be repaired following birth, substantial morbidity and mortality result from pulmonary hypoplasia (PH) and persistent pulmonary hypertension of newborn (PPHN).

The management of CDH has evolved a great deal over time. Initially, CDH was seen as a surgical emergency, requiring immediate reduction of abdominal viscera and repair of the diaphragmatic defect to allow for normal ventilation[3]. However, this approach was associated with greater than 80% mortality[4]. A shift in paradigm occurred in the 1980s with reports of worsening respiratory compliance and pulmonary hypertension following surgical repair[5, 6]. Multiple factors have been suggested for respiratory deterioration following surgery. These include pulmonary vasospasm secondary to stress, increased intra-abdominal pressure associated with reduction of herniating organs and abnormal respiratory mechanics[7]. Today, the treatment of CDH involves early stabilization in an intensive care unit followed by delayed surgical repair. With this approach survival of children born with CDH has improved to greater than 80%[8, 9].

Early stabilization has also evolved over the past three decades. Initially children with CDH were treated with aggressive ventilation in an attempt to improve oxygenation of hypoplastic lungs and to reduce pulmonary hypertension through induced respiratory

alkalosis[10, 11]. However, the fragile lungs of CDH patients were particularly susceptible to over-distention, leading to iatrogenic lung injury. Wung *et al*. first described gentle ventilation with permissive hypercapnia for treatment of infants with severe respiratory failure in 1985[12]. Using this approach, airway pressures were minimized while tolerating a certain degree of respiratory acidosis. This strategy has been adopted in preoperative stabilization of patients with CDH leading to improved survival compared to historical controls[13, 14]. Over time, ventilation strategies have become more sophisticated with the addition of high frequency oscillatory ventilation (HFOV), inhaled nitric oxide (iNO) and extracorporeal membrane oxygenation (ECMO). Today, around one-third of neonates with CDH are treated with ECMO, for whom short-term survival is near 50%[15, 16]. While advances in critical care have improved short-term survival, long-term morbidity remains a major challenge in the management of CDH. In one review from the United Kingdom, 58% of neonates treated with ECMO survived to hospital discharge. Of these only 37% were alive beyond age 1 and only 25% were free of significant morbidity[17].

The prognosis of patients born with CDH depends on the degree of pulmonary hypoplasia and presence of associated congenital anomalies (e.g. heart defects). Since the 1980s a great deal of research has focused on prenatal interventions that might attenuate PH and PPHN. The first successful case report of open fetal surgery for CDH was published in 1990[18]. The technique was eventually abandoned due to a high rate of fetal mortality, mainly from the consequences of premature delivery. Fetal tracheal occlusion was proposed as an alternative based on animal studies. Airway obstruction can induce fetal pulmonary growth by preventing normal outflow of lung fluid. Tracheal occlusion was initially accomplished by means of external clips placed through open or fetoscopic

neck dissection. Fetoscopic surgery was associated with fewer preterm deliveries and hence better survival. However, a number of survivors suffered from tracheal complications, including recurrent laryngeal nerve damage[19]. The technique once again evolved from external clipping to internal occlusion using a detachable balloon placed by means of fetal bronchoscopy through a single port. The first randomized controlled trial of fetal endoscopic tracheal occlusion (FETO) was stopped early in 2003 due to a lack of benefit compared to standardized postnatal care[20]. Despite this setback, interest in FETO continues. Infants with moderate to severe pulmonary hypoplasia are most likely to benefit from FETO. These patients are identified based on their lung-to-head ratio and liver position on fetal ultrasound or magnetic resonance imaging (MRI). A smaller lung-to-head ratio (<1) and liver-up position are associated with a worse prognosis.

Given the risks of fetal surgery, in utero drug therapy is an attractive alternative. Currently this approach is only at an experimental stage in animal models. For example, Larson *et al.* found that in utero overexpression of cystic fibrosis transmembrane conductance regulator (*Cftr*) gene can attenuate PH in the nitrofen model of CDH[21]. Overexpression of CFTR has a general effect on lung epithelial differentiation and it is not known whether this plays a role in the pathogenesis of CDH. Development of more targeted therapies is therefore desired and is the ultimate goal of our research. Achieving this goal requires a better understanding of the pathophysiology of CDH and its effects on lung development.

1.2. Pathophysiology of CDH

1.2.1. Anatomy

Anatomically, CDH is a heterogeneous disease. The defect can occur anywhere in the diaphragm. A Bochdalek hernia is a posterolateral defect, which accounts for approximately 70% of the cases. In about 80% of cases the defect occurs on the left side. The severity of lung disease is correlated to the size of the hernia. On prenatal imaging this is assessed by calculating the lung-to-head ratio and liver position (up or down). Diaphragmatic agenesis occurs in about 14% of neonatal cases and represents the most severe form of CDH. In the modern era, these patients have a mortality rate of greater than 50% and have the highest risk of requiring ECMO, resulting in long-term morbidity[22].

1.2.2. Pulmonary Hypoplasia

Developmentally, PH is characterized by reduced airway branching and decreased gas exchange surface area. Several animal models exist to study pulmonary hypoplasia associated with CDH[23]. In the surgical model, a diaphragmatic defect is created during fetal development in either sheep or rabbit. Pulmonary hypoplasia then occurs secondary to the mass effect of the herniating abdominal organs. The surgical model has been particularly useful for evaluating interventional therapies including prenatal surgery and FETO. On the other hand, since the diaphragmatic defect is created artificially, the surgical model does not reflect the pathogenesis of human CDH.

In the rat model, pregnant dams are given an oral dose of nitrofen, a herbicide, on embryonic day (E) 9 of gestation. Subsequently, around 70% of their offspring will develop CDH and other congenital anomalies, including heart defects. In this model

pulmonary hypoplasia begins prior to the formation of a diaphragmatic defect and continues in lung explants treated with nitrofen *ex vivo*[24]. Based on these observations a dual-hit hypothesis for CDH has been proposed, in which PH starts prior to formation of the diaphragmatic defect and is further exacerbated by herniating abdominal organs. Of note, mutations that result in agenesis of lungs are not associated with CDH, indicating that pulmonary hypoplasia is not the cause of CDH. It is more likely that PH and CDH share a common pathway. For example, children with Fryns syndrome have pulmonary hypoplasia with or without CDH[25].

1.2.3. Persistent Pulmonary Hypertension

Pulmonary hypertension in CDH results from a combination of underdevelopment, meaning reduced total cross sectional area of pulmonary vasculature, as well as maldevelopment, referring to abnormal thickening of pulmonary arterioles. Pulmonary hypertension is further exacerbated by reactive vasoconstriction resulting from post-delivery hypoxemia and acidosis. Little is known about the pathogenesis of PPHN in CDH. The severity of pulmonary hypertension is correlated to the degree of pulmonary hypoplasia, suggesting a common contributing factor.

PPHN is conventionally treated with inhaled nitric oxide, which induces local vasodilation through activation of the endothelial nitric oxide pathway. Although iNO is sometimes used to treat pulmonary hypertension in CDH, it has never been shown to be effective[26, 27]. In the sheep model of CDH, resistance to iNO is at least partly due to altered activity of downstream targets of nitric oxide including guanylate cyclase[28, 29]. Underdevelopment of the vasculature is another reason for resistance to conventional therapy.

1.3. Embryology of the Diaphragm and the Lungs

1.3.1. Normal Development of Diaphragm

In humans, the diaphragm begins to develop at around 4 weeks of gestation[30]. Traditionally the diaphragm is believed to form from the fusion of three embryologic structures: the septum transversum, the esophageal mesentery and the pleuro-peritoneal folds (PPFs). The septum transversum is an infolding of the ventral body wall that gives rise to the anterior portion of the diaphragm. The PPFs are an infolding of the lateral cervical wall that form the posterolateral segments of the diaphragm on either side of the esophageal mesentery. Recent studies in the rat model of CDH indicate that PPFs contribute to the largest portion of the diaphragm. Malformations of the mesenchymal tissue within the PPFs lead to the most common form of CDH, namely a Bochdalek hernia[31, 32].

1.3.2. Stages of Lung Development

In humans, the lung anlage originates from the ventral surface of the primitive foregut around 5 weeks of gestation. The trachea then undergoes bifurcation and branches off the esophagus at around 6 weeks of gestation. From there on, the bronchial tree undergoes a series of elongation and branching steps to form the structures of the conducting airways. In humans, branching of the first 16 generations of the airways is stereotypical and is completed by 16 weeks of gestation. The branching of the last 7 generations is non-stereotypical and is completed by 24 weeks of gestation. In mice, there are only 12 airway generations resulting in 4 lobes on the right and 1 lobe on the left. The 3-dimensional branching pattern of the mouse lung has recently been described in great detail, revealing a remarkably stereotypical geometry. This complex structure is created

by three simple modes of branching, namely domain branching, planar bifurcation and orthogonal bifurcation, that alternate through time[33]. When errors in branching occur they do not seem to affect the future branching pattern, suggesting that the genetic control of lung morphogenesis relies on the repeated use of the same branching mechanisms.

Histologically, lung development has been divided into four stages (Table 1)[34]. During the pseudoglandular stage the epithelial tube, lined with cuboidal cells, undergoes stereotypical branching. At this stage the lung resembles an endocrine gland and is fairly undifferentiated. The canalicular stage is heralded by the formation of distal airway bronchioles accompanied by proximal to distal epithelial differentiation. Concurrently, the mesenchymal layer undergoes differentiation into chondrocytes, fibroblasts and myofibroblasts. Terminal saccules develop during the saccular stage. Epithelial cells begin to differentiate into type I and type II pneumocytes. The mesenchymal layer undergoes apoptosis and extensive vascularization. In the final stage, alveolarization occurs through septation of saccules leading to a honeycomb appearance and substantial increase in the gas exchange surface area. In humans, the alveolar stage begins during the late fetal period and continues into childhood. In rodents, alveolarization is predominantly postnatal.

Table 1. Stages of lung development (E: embryonic day)

Stage	Human age	Rat age
Pseudoglandular	5-17 weeks	E11-17
Canalicular	16-25 weeks	E18-19
Saccular	24-38 weeks	E20-term
Alveolar	38 weeks – 7 years	Postnatal

1.4. Molecular Regulation of Lung Branching Morphogenesis

Normal lung development requires a coordinated crosstalk between epithelial cells and their surrounding mesenchyme. Signaling molecules secreted by the mesenchyme guide epithelial growth and branching. As the epithelial tube grows, it directs differentiation of the surrounding mesenchyme into specialized supporting structures such as airway smooth muscle cells and capillary networks. An essential component of lung branching morphogenesis is the formation of a distal epithelial phenotype. These "tip" cells are at the leading edge of the growing epithelial tube and have the ability to proliferate and grow into the surrounding tissue. A multitude of signaling molecules and transcription factors have been identified that play a role in lung organogenesis. Here I will focus on the most-studied biochemical regulators of lung branching morphogenesis.

Sonic hedgehog (SHH) is an evolutionary conserved signaling pathway involved in the formation of segmented structures. *Shh* is expressed in lung epithelium with higher levels in the terminal buds[35]. Homozygous *Shh*-null mice have profound lung hypoplasia associated with increased apoptosis and reduced proliferation of epithelial and mesenchymal cells. The receptor for SHH is a transmembrane protein called patched (PTC). During lung development *Ptc* expression is highest in the mesenchyme underlying terminal buds. Interestingly, overexpression of *Shh* using a surfactant protein C (SP-C) promoter also results in lung hypoplasia. This phenotype is associated with increased expression of *Ptc* in the mesenchyme and enhanced mesenchymal and epithelial cell proliferation leading to interstitial thickening[36]. These observations indicate that the SHH pathway is involved in regulating cell proliferation through epithelial-mesenchymal interactions and its proper function requires an optimal dose.

The fibroblast growth factor (FGF) family consists of a large group of growth factors involved in many biological processes including angiogenesis, wound healing and embryonic development. FGF10 is an important member of the FGF family that is required for normal development of multiple organs including the brain, lungs and limbs. In lung, FGF10 is a mesenchymal factor that induces epithelial proliferation and migration. Isolated lung endoderm will grow towards a bead coated with FGF10 *in vitro*[37]. In early lung development FGF10 expression is concentrated in the distal mesenchyme surrounding the tips of the elongating bronchi. *Fgf10*-null mice develop a normal trachea, but fail to undergo branching morphogenesis including division of the trachea into main-stem bronchi[38].

Another important ligand in lung development is transforming growth factor beta (TGF-β). There are three isoforms of TGF-β and these all have a different localization during lung development. TGF-β1 is expressed throughout the lung mesenchyme, with higher expression in the distal mesenchymal tissue underlying epithelial branch points. TGF-β2 is localized to the distal epithelium, while TGF-β3 is mainly expressed in the mesothelium and the proximal mesenchyme[39]. Bone morphogenetic protein (BMP) is a member of the TGF-β superfamily. BMP4 plays a central role in distal epithelial proliferation and morphology. FGF10-induced epithelial migration is accompanied by increased expression of BMP4 in the distal epithelium[37]. Blockade of BMP4 or its receptor in lung results in abnormal morphology including reduced epithelial proliferation, extensive apoptosis and formation of large fluid filled spaces[40]. As mentioned previously, lung branching morphogenesis does not occur randomly, but is

stereotypical. Inhibitory molecules control the extent of branching. These include Sprouty (SPRY), an inhibitor of FGF, and Noggin (NOG), a BMP and TGF-β antagonist.

A molecular basis for pulmonary hypoplasia in CDH has not been identified. Chromosomal abnormalities are present in 10% of CDH patients and familial occurrences have been described. However, the majority of cases occur in isolation with no apparent genetic cause[41]. Environmental factors might contribute to the pathogenesis of CDH. In rats, maternal vitamin A deficiency is associated with a high incidence of CDH in pups[42]. In the nitrofen model, administration of vitamin A to pregnant dams reduces the incidence and severity of CDH[43]. Retinoic acid, the biologically active derivative of vitamin A, is essential for early lung development. Acute vitamin A deprivation at the onset of lung development arrests branching morphogenesis, similar to the *Fgf10* knockout mutation[44]. Abnormal retinol levels were found in human cases of CDH independent of maternal retinol status in a small case-control study[45]. Vitamin A deficiency is unlikely to account for all cases of CDH. More likely, retinoic acid might attenuate the phenotype through a related pathway.

The contribution of epigenetics and microRNA (miRNA) to pathogenesis of CDH is unexplored. Epigenetics describes heritable changes in gene expression without alteration of DNA sequence. For example, DNA methylation is a major mechanism underlying cellular differentiation[46]. MicroRNAs are a large group of non-coding small RNA molecules that regulate gene expression through post-transcriptional silencing of messenger RNA (mRNA). MicroRNA function is essential to normal organogenesis during embryonic development. For example, targeted deletion of miR-1-2 results in congenital heart defects in mice[47]. The role of specific miRNAs in the pathogenesis of

human congenital disease is unknown. This project is part of a larger effort to investigate the role of epigenetics and miRNA in the pathogenesis of CDH.

1.5. miRNA and Lung Development

1.5.1. Biogenesis and Function of miRNA

Related miRNAs are often located in a cluster and share the same promoter. There is accumulating evidence that as much as 40% of miRNAs are located within protein coding genes[48]. However, the majority of miRNAs are intergenic and are transcribed as independent units[49]. Initially a long double-stranded primary (pri)-miRNA is synthesized in the nucleus by RNA polymerase II. The pri-miRNA is then processed into a ~70 nucleotide precursor (pre)-miRNA by a ribonuclease III known as Drosha[50]. Drosha is part of a microprocessor complex, which includes a double-stranded RNA binding protein known as Pasha. Pasha acts as an anchor molecule that determines the cleavage site[51].

Upon completion of this nuclear processing step, the pre-miRNA travels through the nuclear pore into the cytoplasm. There, a riboendonuclease III called DICER cleaves the pre-miRNA into a 22-nucleotide double-stranded miRNA. The double-stranded miRNA is then separated into two single strands. The antisense strand participates in the RNA-induced silencing complex (RISC) as a template for target mRNA, while the sense strand is degraded[52]. MicroRNAs mainly bind to the 3' untranslated region (3' UTR) of target mRNAs. Inhibition of gene expression can occur in two ways. In plants, miRNAs base pair with perfect or nearly perfect complementarity to target sequences and inhibit translation by direct destruction or cleavage of mRNA[45]. In animals, miRNAs usually base pair with imperfect complementarity and reduce protein synthesis by inhibiting

translation. RISC can inhibit translation initiation or elongation or cause mRNA instability through deadenylation[53, 54].

1.5.2. miRNA in Lung Development

In one of the first studies to demonstrate the significance of miRNA in lung development, Harris *et al*. created a conditional knockout of the *Dicer* gene in mouse lung epithelium using the SHH promoter shortly after the initiation of lung branching. The mutant lungs demonstrated arrested branching with abnormal expansion of distal epithelial domains[55]. During lung development members of the *Argonaute* (*Ago*) family are localized to branching regions. *Ago1* is mainly localized in the distal epithelium, while *Ago2* is localized in the surrounding mesenchyme[56]. Expression of AGO proteins in several other actively developing regions of the embryo suggests a role for miRNA-mediated dynamic and localized gene regulation. Recently, Dong *et al*. performed a systematic profiling study of microRNA, mRNA, and protein levels during different stages of lung development. They found that while for some miRNAs increased expression directly correlated with down-regulation of predicted mRNA targets; in over half of the proteins analyzed down-regulation occurred independent of changes in mRNA levels. These findings suggest that inhibition of translation without mRNA degradation is an important mechanism of miRNA-mediated gene regulation during lung development[57].

Little is known about the role of specific miRNAs during lung development. It appears that different groups of miRNAs are active at different stages of lung development. miR-17~92 is a cluster of 7 miRNAs that are transcribed as a single pri-miRNA. They were first identified in the pathogenesis of B cell lymphoma and many solid tumors, including lung cancer[58]. Expression of the miR-17~92 cluster is highest in

early stages of lung development, but declines as development proceeds. Overexpression of miR-17~92 using an SP-C promoter results in abnormal lung development characterized by increased epithelial proliferation and reduced differentiation[59]. Deletion of miR-17~92 results in severe lung hypoplasia, but normal branching morphogenesis[60]. Hence, the miR-17~92 cluster is believed to play a crucial role in early lung development by regulating lung cell proliferation and differentiation.

MicroRNA profiling of embryonic lung tissue and lung cancer often produce similar results. As already mentioned, the miR-17~92 cluster is upregulated in both lung adenocarcinomas and during early lung development[61, 62]. In addition, miRNAs with higher expression in adult lung compared to embryonic tissue are downregulated in lung cancer. The best example of this relationship is the let-7 family, which is downregulated in embryonic lung as well as lung tumors compared to normal adult tissue[62]. In human cells, *let-7* negatively regulates RAS protein and is therefore considered to be a tumor suppressor gene[63]. Lu *et al*. investigated the function of miRNAs during the late canalicular stage of lung development. They compared the relative expression of microRNAs between E11.5 (pseudoglandular stage) and E17.5 (late canalicular stage) in mice. The most abundant miRNA at E11.5 was miR-17, while at E17.5, let-7 was the most abundant miRNA[64]. Therefore, transition from early branching morphogenesis to later differentiation is accompanied by a switch from the miR-17~92 cluster to the let-7 family.

1.6. Epithelial-to-Mesenchymal Transition (EMT)

1.6.1. EMT in Development and Disease

Nitrofen-induced CDH is characterized by pulmonary interstitial thickening and increased fibroblast proliferation[65, 66]. One of the objectives of this project is to determine whether epithelial-to-mesenchymal transition contributes to the pathogenesis of nitrofen-induced CDH. Epithelial cells are characterized by an apical-basal polarity. They are held together by cell-cell adhesion molecules and are bound by a basement membrane. These architectural constraints are essential for proper functioning of epithelial tissue as barriers or in absorption. They also lead to the formation of typical epithelial structures, such as sheets, tubes or vesicles. Mesenchymal cells, for example fibroblasts, are characterized by an elongated spindle shape, cellular motility and ability to produce extracellular matrix (ECM). Epithelial-to-mesenchymal transition is a process by which epithelial cells acquire features of mesenchymal cells, namely the ability to lose cell-cell contacts and become mobile and invasive. EMT is essential in early embryonic development. During gastrulation the primordial mesoderm forms from endodermal progenitor cells. These epithelial cells change their shape to a more elongated form, migrate to the midline and extend along an antero-posterior axis[67]. EMT and its reverse process, mesenchymal-to-epithelial transition (MET), occur several times during organogenesis. Examples include development of the neural crest[68], kidneys[69, 70] and heart[71, 72].

EMT has garnered a great deal of interest in the past decade due to its potential role in adult diseases, such as cancer and organ fibrosis. EMT is believed to be one of the main mechanisms by which adenocarcinomas progress to invasion and metastasis. Indeed many inducers and inhibitors of EMT are considered oncogenes and tumor suppressors,

respectively[73]. Idiopathic pulmonary fibrosis (IPF) is a chronic lung disease characterized by progressive interstitial fibrosis. Using a mouse model, Kim *et al*. have shown that the majority of fibroblasts in pulmonary fibrosis arise from alveolar epithelial cells[74]. Similarly in renal fibrosis a substantial number of fibroblasts originate from tubular epithelial cells[75]. Accordingly, markers of EMT are increased in biopsies of patients with IPF and renal fibrosis[74, 76].

1.6.2. EMT Signaling Pathway

Several signaling pathways contribute to activation of EMT. The most important and best-studied mechanism involves TGF-β-induced SMAD signaling. Binding of TGF-β to its transmembrane kinase receptors, TβRI and TβRII, results in phosphorylation of intracellular SMAD molecules. Upon phosphorylation, isoforms of SMAD form trimers that translocate into the nucleus, where they function as coactivators or corepressors of gene expression. The target genes encode transcription factors, such as members of the *Snail* family and *Zeb* family, that enhance expression of mesenchymal proteins, while repressing expression of epithelial proteins[77]. EMT can be detected *in vivo* when epithelial cells cease to express transmembrane adhesion molecules such as E-cadherin and begin to produce mesenchymal cytoskeletal components, such as vimentin.

1.6.3. miR-200 Family Inhibits EMT

MicroRNA-200b is a member of miR-200 family that also includes miR-200a, miR-200c, miR-141 and miR-429. These miRNAs have similar sequences and are transcribed in two clusters: miR-200b, 200a and 429 share a common transcription start site on chromosome 1; while miR-200c and 141 are transcribed as a single unit from chromosome 12[78]. Currently little is known about the role of miR-200b in lung development. Based on

sequence complementarity and experimental data, the miR-200 family inhibit several components of the TGF-β/SMAD signaling pathway including TGF-β, TβR and ZEB[79, 80]. ZEB is a zinc-finger transcriptional repressor of E-cadherin. Overexpression of ZEB can promote EMT, while its downregulation can induce an epithelial phenotype[80, 81]. miR-200b has strong affinity for the 3' UTR of ZEB1 and ZEB2. In adults, miR-200b is expressed in epithelial tissues. Decreased expression of miR-200b leads to EMT through activation of TGF-β/SMAD signaling. On the other hand, increased expression of miR-200b can effectively reverse EMT *in vitro*[82]. The miR-200 family is suppressed in a mouse model of pulmonary fibrosis[83]. In these lungs miR-200b levels are higher in alveolar epithelial cells compared to fibroblasts. In addition, the onset of pulmonary fibrosis is associated with reduced miR-200b expression.

1.7. Rationale for The Project and Objectives

A previous microarray screen, including 319 human miRNAs, in pulmonary tissues from fetuses with CDH found miR-200b to be upregulated nearly 50 fold (unpublished data). This finding led us to hypothesize that miR-200b is important for lung development and that its expression is changed in pulmonary hypoplasia due to CDH. The objectives of this project were to:

1. Develop a robust in situ hybridization (ISH) protocol to investigate the localization of miRNAs in tissue sections
2. Determine the expression pattern of miR-200b in human lungs from CDH patients and rat embryonic lungs with nitrofen-induced CDH, and compare the expression patterns to that in control lungs

3. Use parallel immunohistochemistry (IHC) experiments to propose a model for the role of miR-200b in pulmonary hypoplasia associated with CDH

CHAPTER 2. MATERIALS & METHODS

2.1. Human Neonatal Lung Tissue

Sectioned (5 μm) formalin-fixed, paraffin-embedded newborn lung tissues on microscope slides were kindly provided by professor Dick Tibboel (Department of Pediatric Surgery, Erasmus MC-Sophia, Rotterdam, the Netherlands). Samples had been obtained post-mortem from three infants with CDH and three age-matched controls (Table 2). Slides were given institutional exemption for research purposes. The Research Ethics Board of Erasmus MC-Sophia approved the study protocol.

Table 2. Human tissues used in the study

Age	Control Diagnosis	CDH Diagnosis
35 weeks	Rupture of tentorium cerebelli with severe hemorrhage	Right CDH, both lungs hypoplastic
37 weeks	Heart failure due to a large thrombus in the left myocardial ventricle	Left CDH
40 weeks	Epidural hemorrhage	Right CDH, hypoplastic left lung, agenesis of the right lung

CDH: Congenital Diaphragmatic Hernia

2.2. Rat Fetal Lung Tissue

2.2.1. Nitrofen Model

Ethics approval for the use of animals in research was obtained from the Bannatyne Campus Protocol Management & Review Committee, University of Manitoba. Sprauge-Dawley rats were kept in a controlled light-dark cycle and food and water were supplied

ad libitum. Rats were mated overnight and the finding of a sperm-positive vaginal smear was designated day 0 of gestation. The herbicide 2,4-Dichlorophenyl 4-nitrophenyl ether (nitrofen) was obtained from Sigma-Aldrich Co. (St. Louis, MO, USA). To induce CDH, pregnant dams were given 100 mg of nitrofen dissolved in olive oil by oral gavage on E9. Past experience has shown that up to 80% of the offspring will develop a CDH and 100% will suffer from pulmonary hypoplasia (Figure 1). Control rats were given an equal volume of olive oil without nitrofen. Dams were euthanized by CO2 overexposure following a short isoflurane anesthesia. Fetuses were removed at different stages of lung development (E13, 15, 18 and 21) using microsurgical techniques. At E13, whole embryos were harvested following removal of the head and tail. At E15, only the thorax was preserved. At E18 and E21, the chest was opened via a median sternotomy to check for the presence of a hernia. We also noted the size of the hernia (unilateral vs. agenesis) and the degree of pulmonary hypoplasia. In the nitrofen group, only lungs from fetuses with a CDH were preserved.

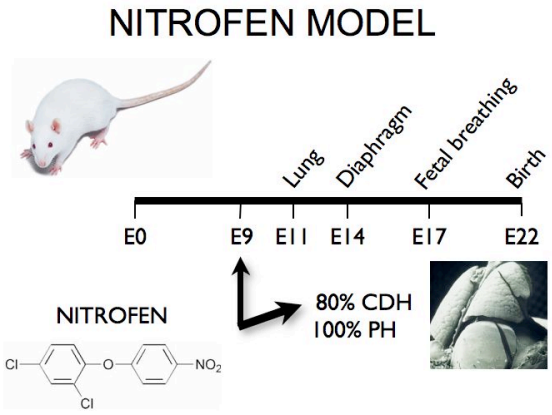

Figure 1. Nitrofen model – Pulmonary hypoplasia (PH) and congenital diaphragmatic hernia (CDH) were induced in rat fetuses by maternal administration of nitrofen on embryonic day (E) 9.

2.2.2. Tissue Processing

Whole fetuses and isolated lungs were fixed with 4% paraformaldehyde (PFA) in phosphate buffered saline (PBS) for 16-18 hours at 4°C. Post fixation, the tissues were dehydrated in a graded alcohol series, cleared in xylene and embedded in paraffin. Serial sections (4 μm-thick) were obtained using a microtome and mounted on SuperFrost microscope slides (Fisher Scientific, Hampton, NH, USA). Three sections were placed per slide to provide a three-dimensional view of the tissue (Figure 2).

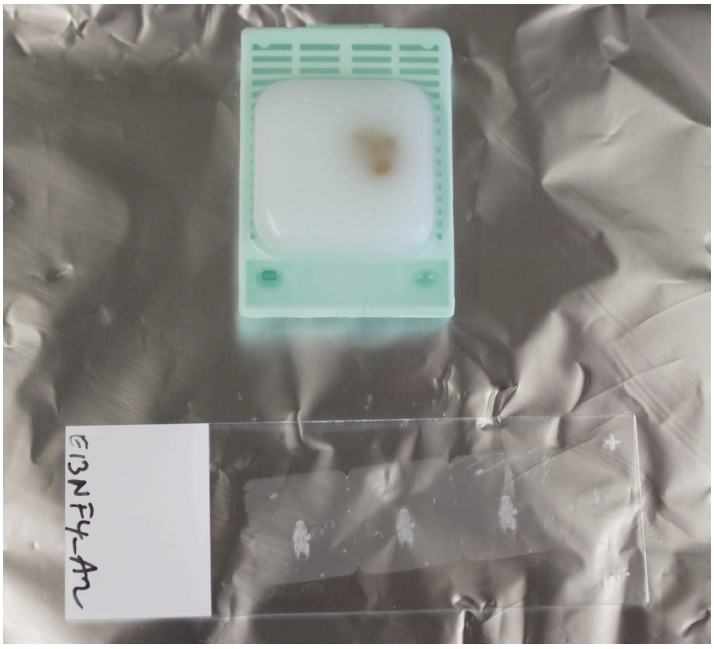

Figure 2. Serial sectioning – Consecutive 4 μm thick sections of lung tissue were mounted on a single microscopic slide to provide a three-dimensional view.

2.3. In Situ Hybridization

A modified one-day in situ hybridization protocol was developed based on a previously described procedure (Figure 3)[84, 85]. All glassware and metallic trays were heated to 180°C for 8 hours to reduce RNase contamination. Pipettes and other instruments were

wiped with RNase AWAY solution (Ambion, Burlington, ON, Canada). Reagents were made with RNase-free water and autoclaved.

The slides were first heated to 58°C for 30 minutes to melt the wax. The sections were then deparaffinized in xylene, rehydrated through an ethanol dilution series (100% to 70%) and transferred to PBS with 0.1% Tween. A hydrophobic barrier was drawn around each section using an ImmEdge pen (Vector Laboratories, Burlington, ON, Canada). Tissues were partly digested with 20 μg/ml of proteinase K at 37°C for 10 minutes to facilitate probe penetration and exposure of miRNA species. The reaction was stopped with 0.2% glycine followed by post-fixation in 4% PFA for 10 minutes. The slides were then washed in PBS twice. Non-specific protein-RNA interactions were eliminated by acetylation (66 mM HCl, 0.66% acetic anhydride and 1.5% triethanolamine), followed by three washes in PBS. Prehybridization was carried out in a sealed chamber humidified with 1X sodium chloride/sodium citrate (SSC) buffer at 50°C for 30 minutes. Hybridization solution consisted of 50% formamide, 5X SSC, 500 μg/ml yeast tRNA and 1X Denhardt's solution. Each miRNA was detected using a specific locked nucleic acid (LNA) probe double-labeled at the 3' and 5' end with digoxigenin (DIG) (Exiqon, Vedbaek, Denmark). Different probes were used for detection of miR-200b in human and rat tissues. A scramble probe was used as negative control and a probe against U6 small nuclear RNA (snRNA) was used as positive control (Table 3). Rat probes were diluted to 50nM and human probes were diluted to 100nM in hybridization solution and applied to sections for 1 hour at 30°C below the predicted RNA melting temperature.

Table 3. Locked nucleic acid probes used for in situ hybridization

Probe	Sequence	Hybridization Temperature
hsa-miR-200b (human)	TCATCATTACCAGGCAGTATTA	52°C
rno-miR-200b (rat)	GTCATCATTACCAGGCAGTATTA	52°C
Scramble-miR (negative control)	GTGTAACACGTCTATACGCCCA	57°C
U6 (positive control)	CACGAATTTGCGTGTCATCCTT	54°C

Post-hybridization, the slides were washed in 5X, 1X and 0.2X SSC buffer at hybridization temperature. The sections were then incubated in a blocking solution containing 1X Roche Blocking Reagent (Roche, Mannheim, Germany), Tris-NaCl buffer (pH 7.5) and 0.1% Tween. DIG-labeled probes bound to target miRNA were detected by a sheep alkaline phosphatase (AP)-conjugated anti-DIG antibody (Roche), diluted 1:250 in blocking solution and incubated at room temperature for 1 hour. Post-antibody, the slides were washed three times in Tris-NaCl buffer and three times in NTM buffer (0.1 M NaCl, 0.1 M Tris-HCl, pH 9.0-9.5 and 0.05 M $MgCl_2$). Chromogenic reaction was carried out in the dark at 30°C for 2 hours using 1-Step NBT/BCIP solution (Thermo Scientific, Waltham, MA, USA) containing 1mM levamisole. Slides were washed in double-distilled water and counterstained with methyl green. At the end, sections were

dehydrated in a graded alcohol series, cleared in xylene and coverslipped under Permount (Fisher Scientific).

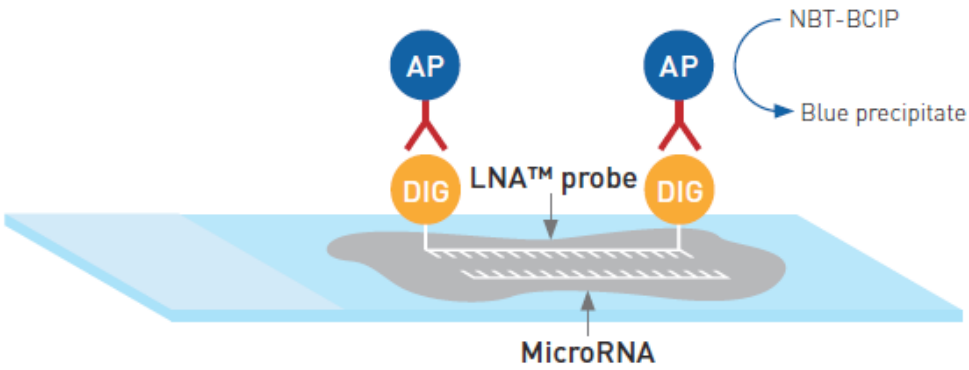

Figure 3. In situ hybridization – MicroRNA in tissue sections was hybridized to a complementary locked nucleic acid (LNA) probe double-labeled with digoxigenin (DIG). The probes were detected by an alkaline phosphatase (AP)-conjugated anti-DIG antibody.

2.4. Immunohistochemistry

IHC was performed using the VECTASTAIN ABC system from Vector Laboratories[86]. Between each step, sections were washed three times in PBS. Tissues were first deparaffinized and rehydrated as described above. Antigen unmasking was achieved using citrate buffer (pH 6.0) in a boiling water bath over 30 minutes. Slides were allowed to cool to room temperature and were blocked with a solution containing 10% goat serum, 1X Roche Blocking Reagent and 0.1% Tween in PBS. Endogenous peroxidase activity was eliminated by treatment with 3% hydrogen peroxide for 30 minutes. Endogenous avidin and biotin molecules were blocked using the avidin/biotin blocking kit. Tissues were then incubated with a rabbit monoclonal anti-vimentin antibody (Abcam Inc., Cambridge, MA, USA) diluted 1:500 in blocking solution at 4°C overnight. The

secondary antibody consisted of a biotinylated goat anti-rabbit antibody (Jackson Laboratories, West Grove, PA, USA) diluted 1:400 in blocking solution. Tissues were incubated with the secondary antibody at room temperature for 30 minutes. The ABC kit was used to bind avidin-conjugated horseradish peroxidase (HRP) to the biotinylated secondary antibody. Chromogenic reaction was carried out using the ImmPACT DAB substrate (Vector Laboratories) for 30 seconds. Slides were washed in double-distilled water and counterstained with methyl green (Thermo Scientific, Rockford, IL, USA). At the end, sections were dehydrated in an alcohol series, cleared in xylene and coverslipped under Permount.

2.5. Image Analysis

Digital microscopy was performed using the ScanScope CS system (Aperio, Vista, CA, USA). Images were obtained up to 200X magnification and were viewed and analyzed with ImageScope software (http://www.aperio.com). The area of ISH staining was quantified using the colocalization algorithm[87]. The blue and green stains were first calibrated with the color deconvolution tool using positive (U6 probe without counterstain) and negative (scramble probe with methyl green counterstain) control slides, respectively. The average optical densities of each stain in the red, blue and green channels were then entered into the colocalization algorithm. The program creates a digital map of the slide made up of three colors: blue, green and aqua. Aqua denotes colocalized positive and negative staining. This digital map was visually checked against the original image to ensure accuracy. The software outputs the area of each color as a percentage of all three colors. Positive staining was calculated by adding the percentages of blue and aqua (% positive staining).

For human samples and E15, E18 and E21 rat embryos the entire lung was analyzed. For E13 rat embryos, a line drawn around the epithelial tube and the surrounding mesenchymal layer defined the area of analysis.

2.6. Statistical Analysis

Each comparative group consisted of three embryos and for each embryo three sections were analyzed (n =9). All data are presented as mean ± standard error of mean. When comparing two groups, *p* values were calculated by the two-tailed Student's *t* test. When comparing three groups, one-way ANOVA with Tukey-Kramer multiple comparisons test was utilized. $P < 0.05$ was selected for acceptance of statistical significance.

CHAPTER 3. RESULTS

3.1. Evaluation of the ISH Protocol

The ISH protocol was first tested on E21 rat tissue using U6 and scramble probes (Figure 4). The staining became darker with increasing concentrations of U6. Incubation with the scramble probe resulted in no appreciable signal.

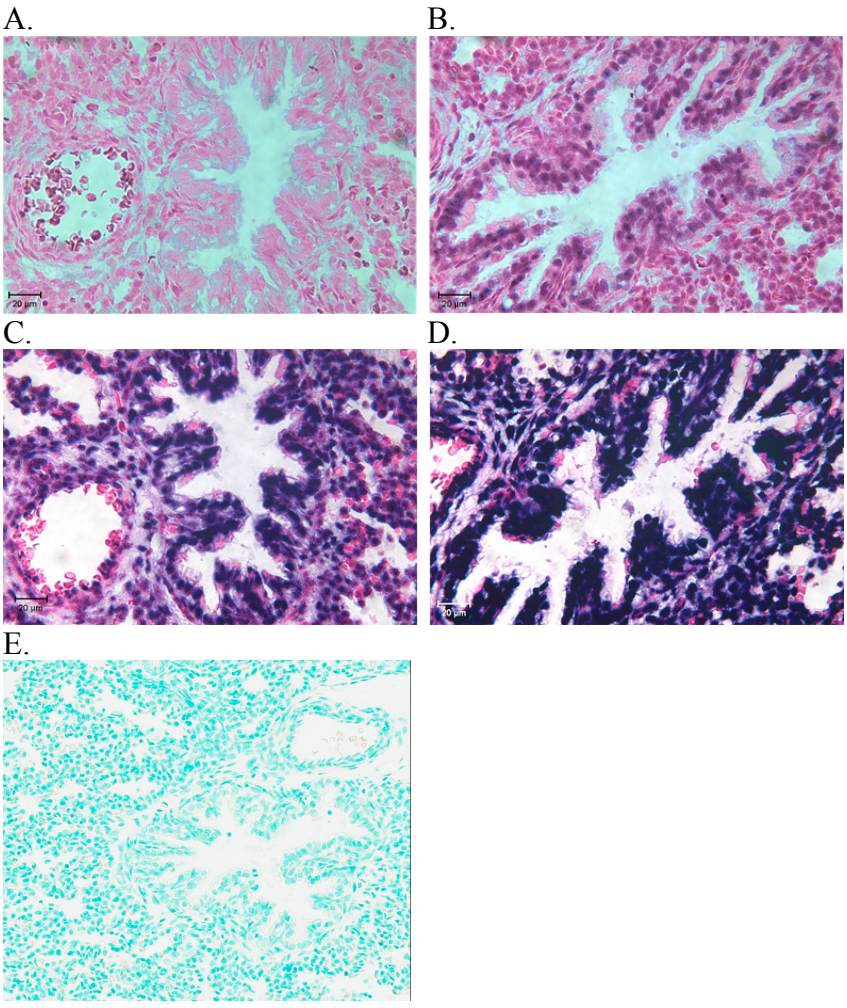

Figure 4. Evaluation of ISH protocol – A. no probe, B. 0.03 nM, C. 0.1 nM and D. 0.5nM U6 snRNA (counterstained with nuclear fast red; 400X magnification). E. Scramble probe at 50 nM (counterstained with methyl green; 200X magnification).

3.2. Human Neonatal Lung

In situ hybridization of human neonatal lung revealed a specific spatial and cellular distribution of miR-200b. In conducting airways, epithelial cells were positive for miR-200b, while parabronchial smooth muscle cells were negative. In CDH lungs, terminal saccules were characterized by thickened septa with an increased number of miR-200b-positive cells (Figure 5). When entire lung sections were analyzed, miR-200b levels were higher in CDH patients compared to controls (Figure 6).

Control

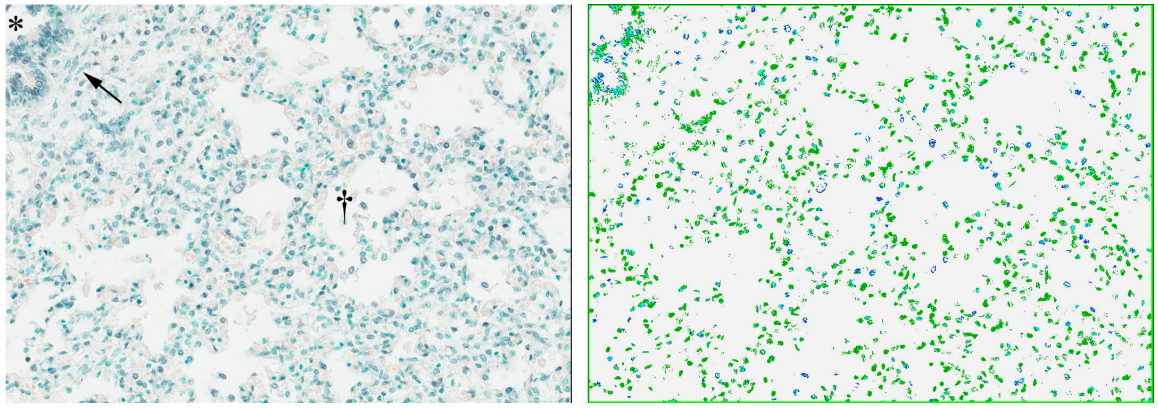

CDH

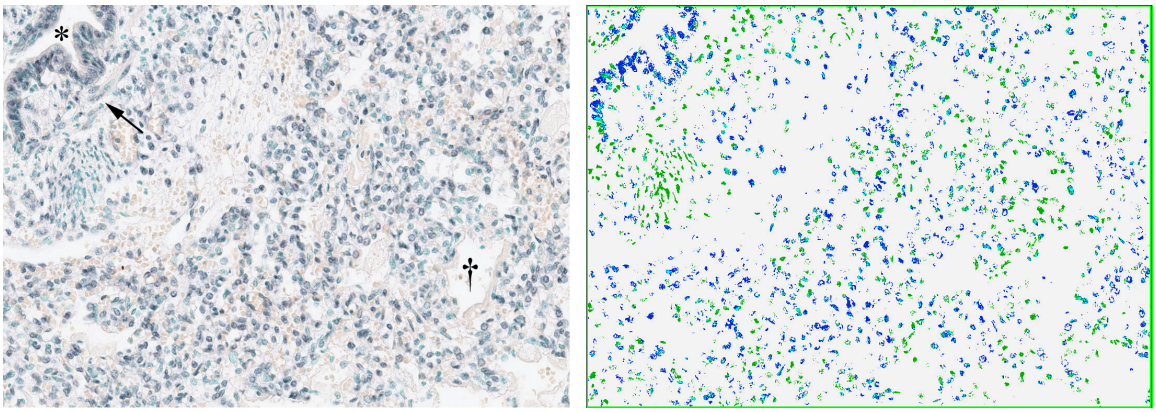

Figure 5. Distal expression of miR-200b (blue stain) in human neonatal lung (200X magnification) – Original images (left) and their corresponding color-coded maps (blue = positive staining, green = negative staining, aqua = colocalized positive and negative staining). Bronchial epithelial cells are positive for miR-200b (*), while parabronchial

smooth muscle cells are negative (arrow). In CDH lungs, terminal saccules (†) are characterized by thickened septa with increased number of miR-200b-positive cells.

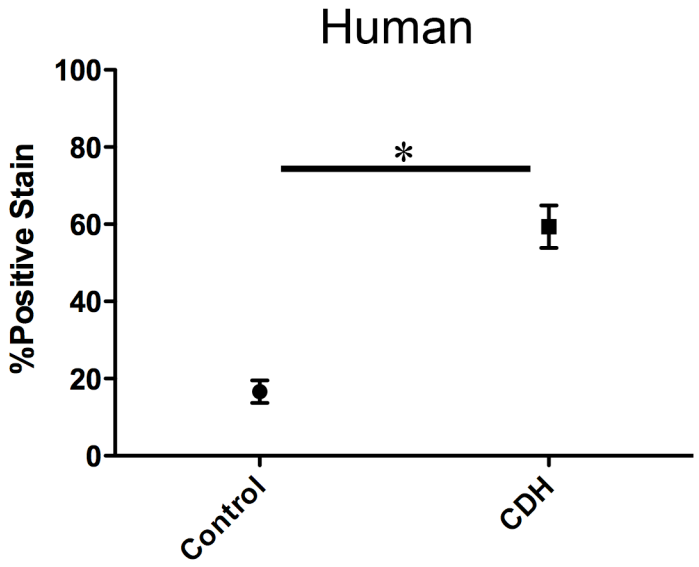

Figure 6. Area of ISH staining for miR-200b in human neonatal lung (*P <0.0001).

3.3. Rat Fetal Lung

3.3.1. Pseudoglandular Stage (E13-E15)

In the pseudoglandular stage of lung development, miR-200b expression was highest at the tips of the growing bronchial tree. This was confirmed by serial sectioning (Figure 7). The splanchnic mesenchyme was positive for miR-200b except for the immediate layer adjacent to the epithelial tube. This parabronchial mesenchyme became positive more distally and surrounding the elongating tips. Nitrofen-treated lungs had lower miR-200b expression, particularly in the distal epithelium and its surrounding mesenchyme (Figures 8 and 9). When entire lung sections were analyzed, nitrofen-treated rats had lower expression of miR-200b compared to controls (Figures 10 and 11).

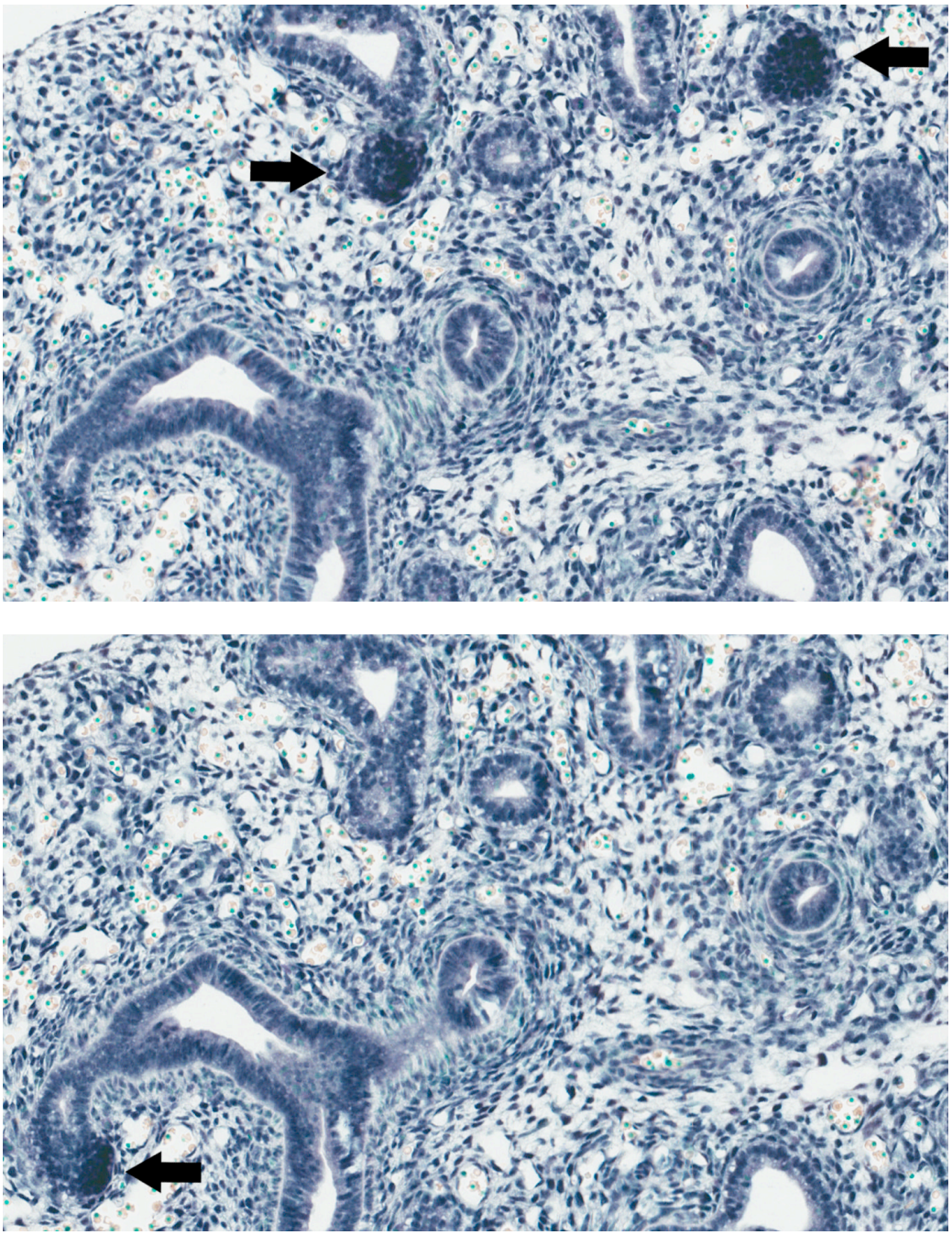

Figure 7. miR-200b expression (blue stain) is highest at the tips of the elongating bronchial tree (arrows). Serial sections of E15 control rat lung (200X magnification).

Control

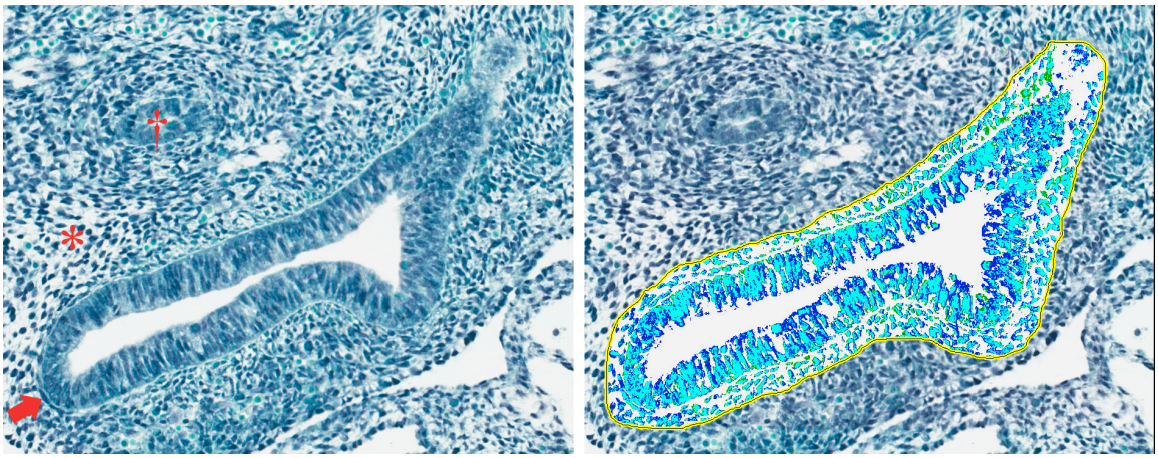

Nitrofen

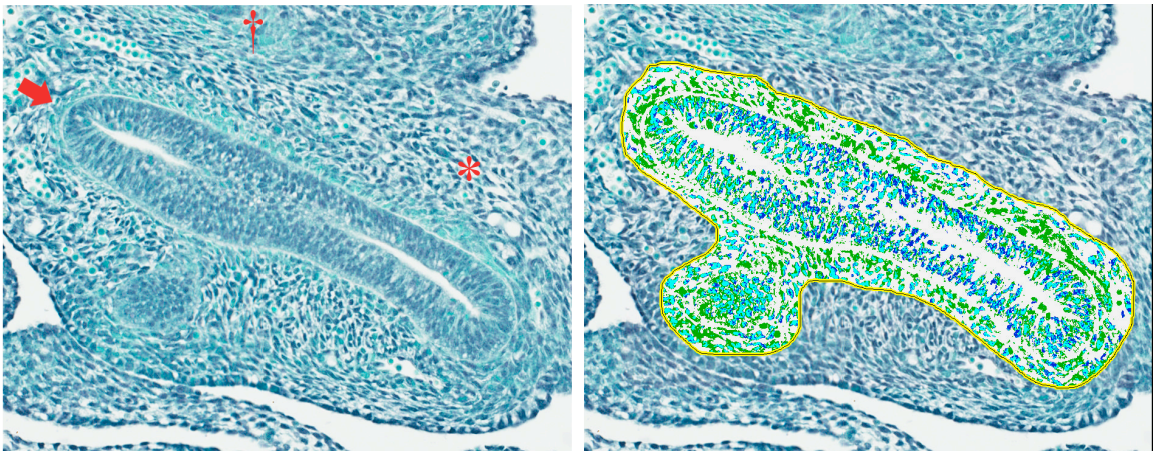

Figure 8. ISH for miR-200b (blue stain) in E13 rat lung (200X magnification) – Original images (left) and their corresponding color-coded maps (blue = positive staining, green = negative staining, aqua = colocalized positive and negative staining). Undifferentiated splanchnic mesenchyme (*) is positive for miR-200b. In control lungs, distal parabronchial cells (arrow) are positive for miR-200b, while proximal parabronchial cells are negative. In nitrofen-treated lungs, both distal and proximal parabronchial cells are negative for miR-200b. Esophagus (†).

Control

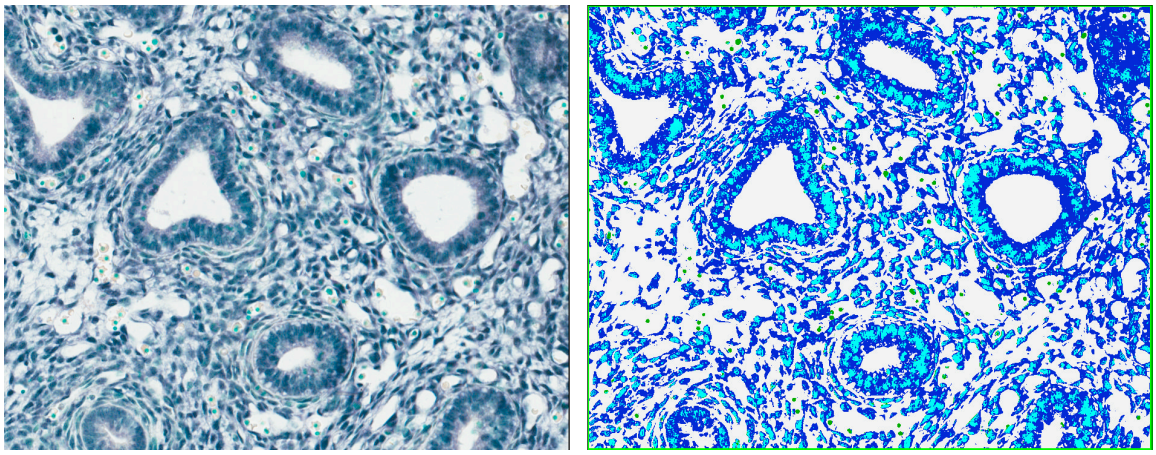

Nitrofen

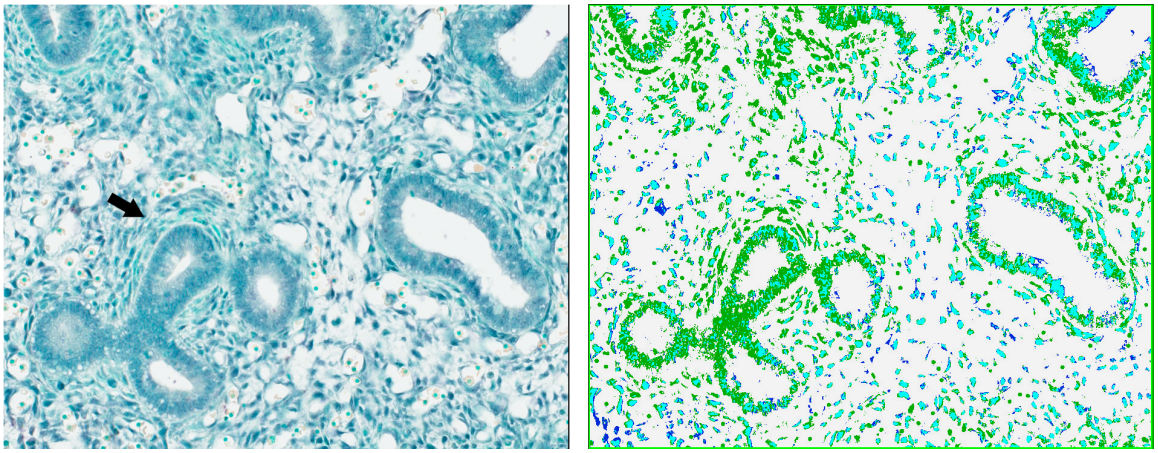

Figure 9. Distal expression of miR-200b (blue stain) in E15 rat lung (200X magnification) – Original images (left) and their corresponding color-coded maps (blue = positive staining, green = negative staining, aqua = colocalized positive and negative staining). In control lungs the majority of cells are positive for miR-200b. Nitrofen-treated lungs have lower expression of miR-200b, especially in parabronchial tissue (arrow).

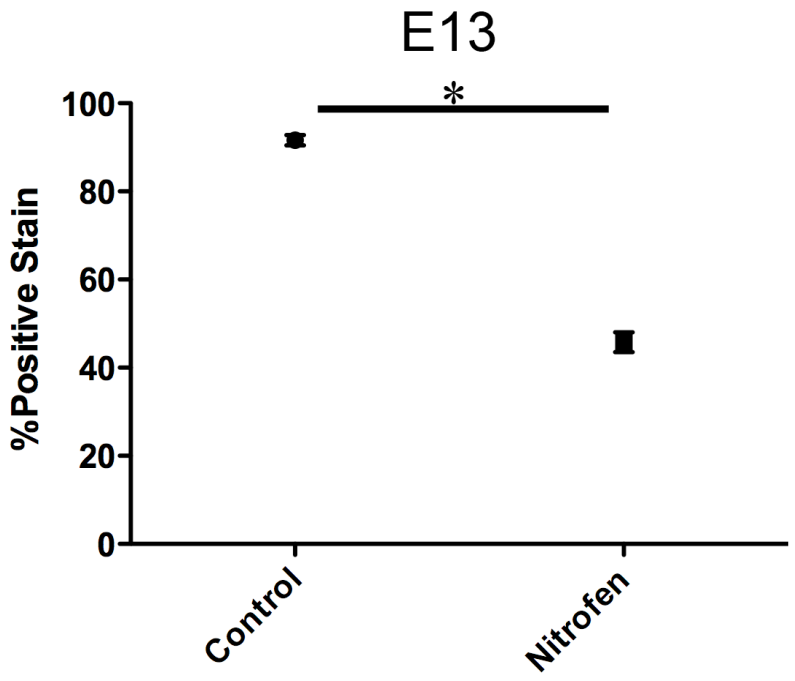

Figure 10. Area of ISH staining for miR-200b in E13 rat lung (*P <0.0001).

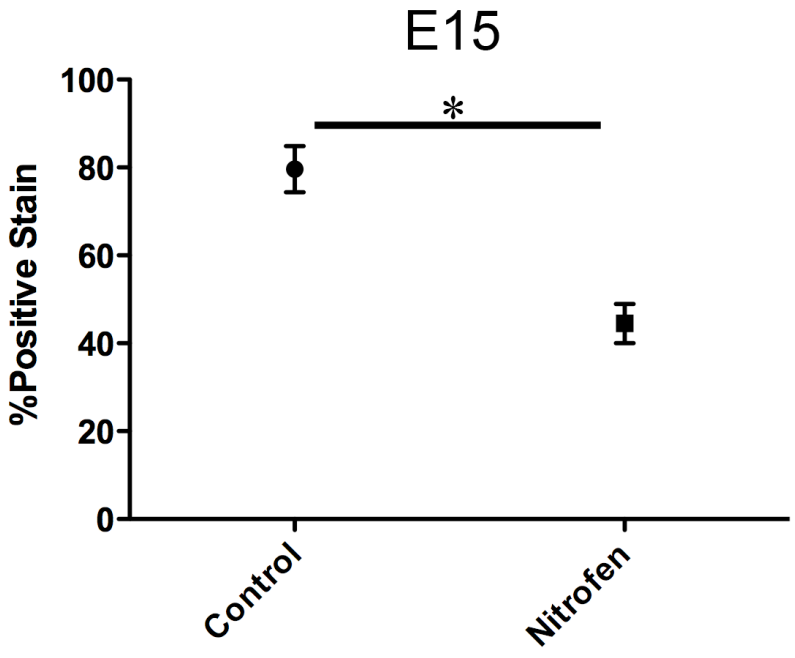

Figure 11. Area of ISH staining for miR-200b in E15 rat lung (*P =0.0001).

3.3.2. Canalicular Stage (E18)

In the canalicular stage, relative to the pseudoglandular stage, expression of miR-200b was decreased in the pulmonary mesenchymal tissue. High expression of miR-200b continued in the distal tips of the elongating bronchioles. CDH lungs had lower expression of miR-200b in both mesenchymal and epithelial layers (Figure 12). In addition, there were fewer tip structures per area of the lung in hypoplastic lungs.

In blood vessels, endothelial cells stained positive for miR-200b, while the surrounding smooth muscle layer was predominantly negative. In CDH rats, endothelial cells were mostly negative for miR-200b. Mesothelial cells were strongly positive for miR-200b in both control and CDH rats (Figure 13). This pattern continued into the saccular stage. When entire lung sections were analyzed, CDH rats had lower expression of miR-200b compared to controls (Figure 14).

Control

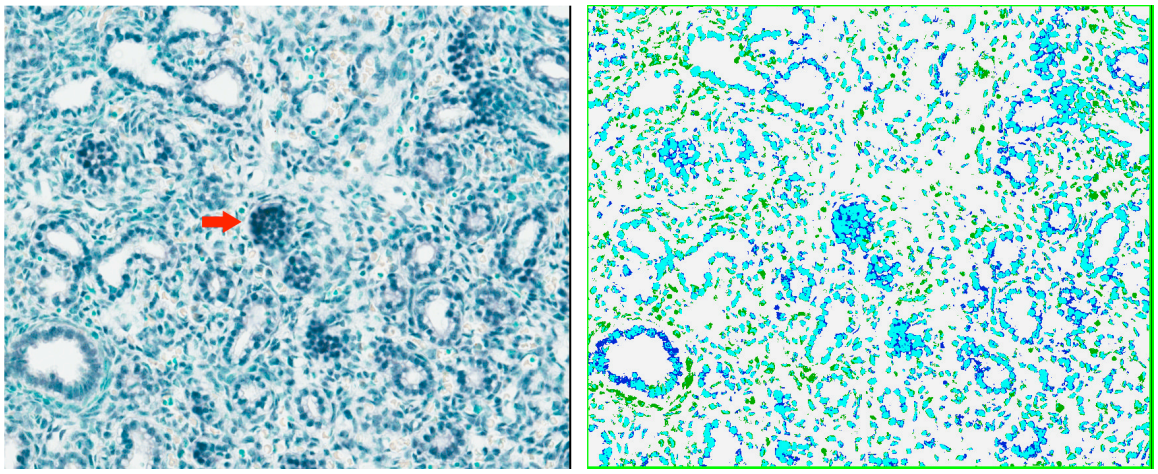

CDH

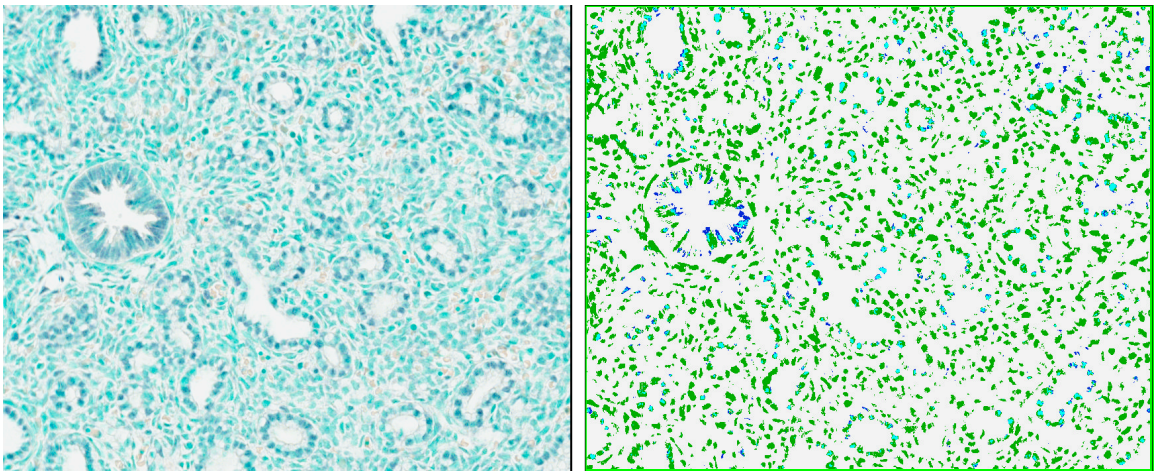

Figure 12. ISH for miR-200b (blue stain) in E18 rat lung (200X magnification) – Original images (left) and their corresponding color-coded maps (blue = positive staining, green = negative staining, aqua = colocalized positive and negative staining). CDH lungs have lower expression of miR-200b and contain fewer tip structures (arrow in control lung).

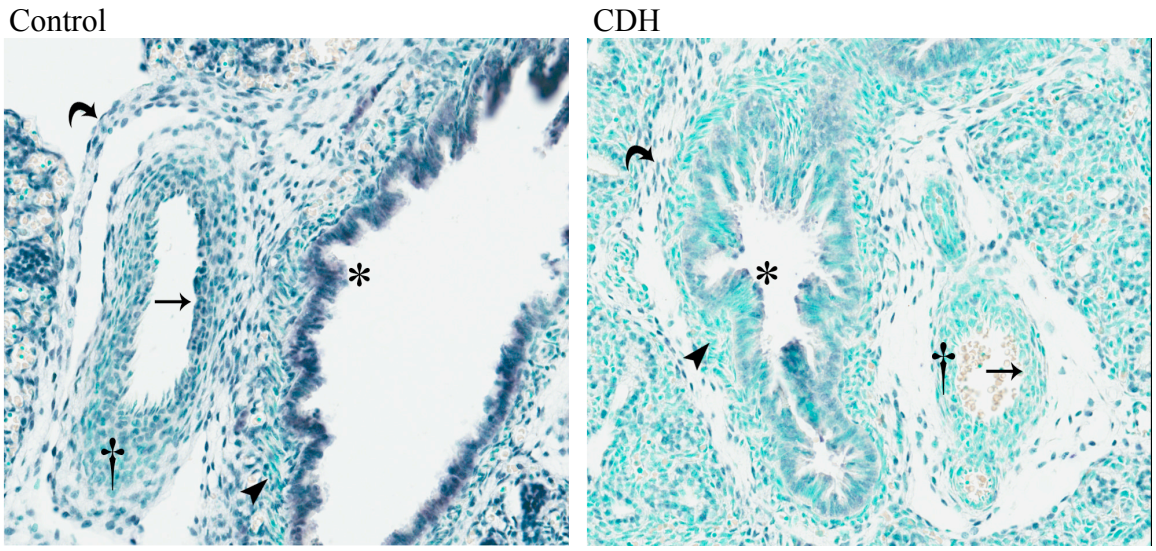

Figure 13. Proximal miR-200b expression (200X magnification) – Bronchial epithelial cells are positive for miR-200b (*), while parabronchial cells are negative (arrow head). In blood vessels, endothelial cells are positive for miR-200b (straight arrow), while the surrounding smooth muscle layer is negative (†). In CDH lungs endothelial cells were predominantly negative for miR-200b. Mesothelial cells are positive in both control and CDH lungs (curved arrow).

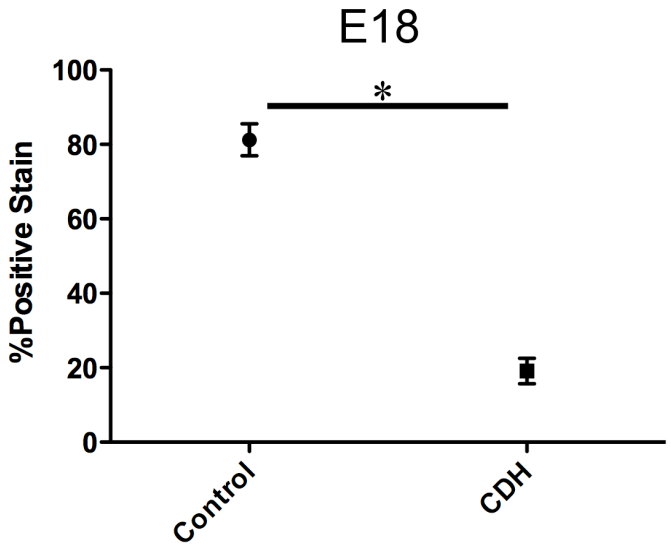

Figure 14. Area of ISH staining for miR-200b in E18 rat lung (*P <0.0001).

3.3.3. Saccular Stage (E21)

The spatial and cellular distribution of miR-200b in the saccular stage was similar to human tissue as described above. Expression of miR-200b was higher in the epithelial cells of proximal airways compared to distal bronchioles and terminal saccules (Figure 15, blue vs. aqua in color-coded maps). In terminal sacs, cells facing the luminal side were predominantly positive for miR-200b. On the other hand, negative cells were more often found within the walls of the sacs.

At E21 60% of the offspring treated with nitrofen developed CDH. In the hernia group two distinct phenotypes were recognized: a mild phenotype associated with a small unilateral hernia and a severe phenotype associated with diaphragmatic agenesis. The severe phenotype had much lower expression of miR-200b in terminal saccules, where there was an increase in the number of green cells (Figure 15). When both phenotypes were combined, CDH lungs had lower expression of miR-200b compared to control lungs (Figure 16). When analyzed separately, the difference between control lungs and the mild phenotype was not statistically significant. Both control lungs and the mild phenotype had higher expression of miR-200b compared to the severe phenotype (Figure 17).

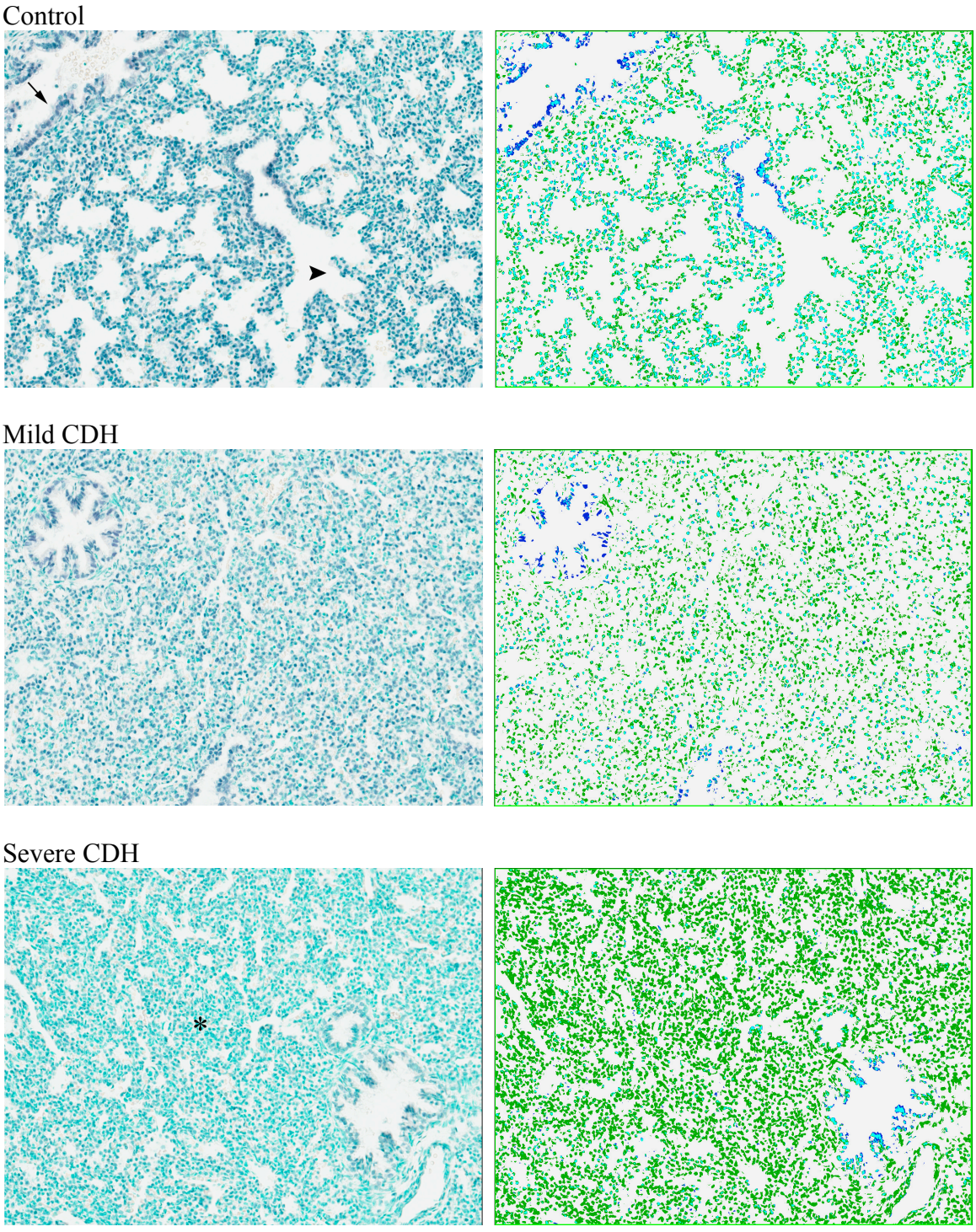

Figure 15. ISH for miR-200b (blue stain) in E21 rat lung (200X magnification) – Original images (left) and their corresponding color-coded maps (blue = positive staining, green = negative staining, aqua = colocalized positive and negative staining). Expression

of miR-200b is higher in proximal airways (arrow) compared to terminal saccules (arrow head). The severe CDH phenotype is characterized by abundance of miR-200b-negaive cells in terminal saccules (*).

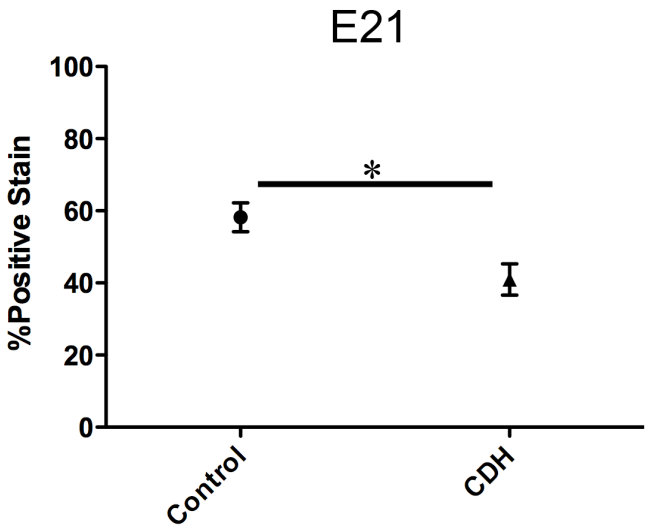

Figure 16. Area of ISH staining for miR-200b in E21 rat lung with all CDH lungs combined (*P =0.0174).

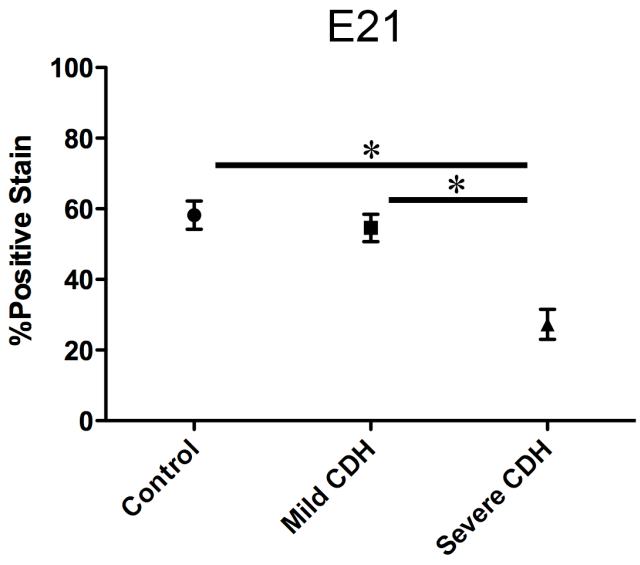

Figure 17. Area of ISH staining for miR-200b in E21 rat lung with CDH lungs separated into mild and severe phenotypes (*P <0.001).

3.3.4. Immunohistochemistry

To further explore the role of EMT in lung development, the spatial and temporal expression of vimentin in embryonic rat pulmonary tissue was determined through IHC. Vimentin was expressed in mesenchymal tissue throughout lung development. In the pseudoglandular stage vimentin was also expressed in distal, but not proximal epithelium (Figures 18 and 19). This pattern continued into the canalicular stage. In the saccular stage vimentin was absent from epithelial cells and was found exclusively in mesenchymal tissue.

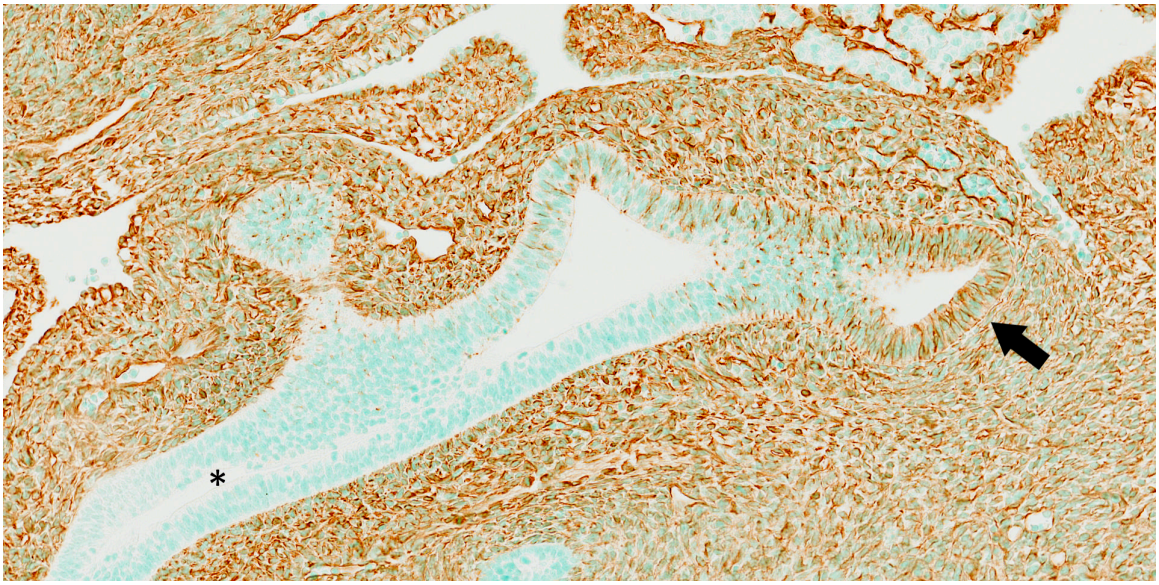

Figure 18. Immunohistochemistry for vimentin (brown stain) in E13 rat lung. Vimentin is expressed in the distal epithelium (arrow), but is absent from the proximal epithelium (*) (200X magnification).

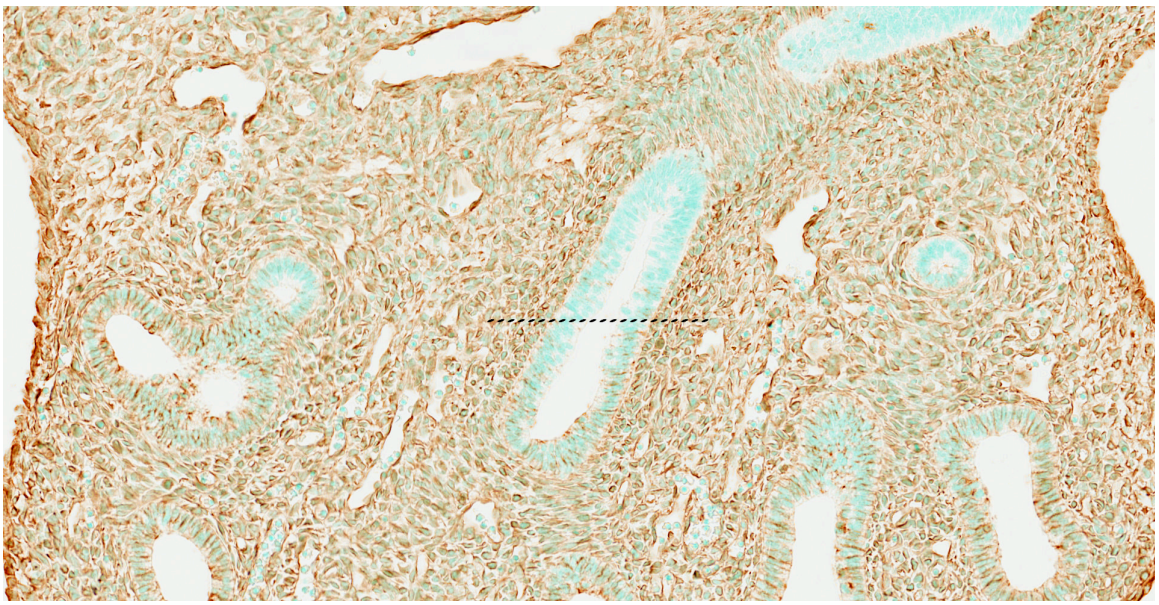

Figure 19. Immunohistochemistry for vimentin (brown stain) in E15 rat lung. Vimentin is expressed in the distal epithelium below the dashed line, but is absent in the proximal epithelium above the dashed line (200X magnification).

CHAPTER 4. DISCUSSION

4.1. miR-200b & Mesenchymal Differentiation

The pattern of ISH staining suggests that expression of miR-200b during lung development parallels cellular differentiation (Figure 20). In mesenchymal tissue, miR-200b expression decreases with increasing differentiation (e.g. into myofibroblasts). In early pseudoglandular stage (E13), miR-200b is expressed widely in the undifferentiated splanchnic mesenchyme. In parabronchial tissue, which is differentiating into airway smooth muscle, a distal-to-proximal gradient is observed (Figure 8). In control lungs, distal parabronchial cells are strongly positive for miR-200b, while proximal parabronchial cells are negative. Mailluex *et al*. have shown that distal parabronchial cells are smooth muscle progenitors that express high levels of FGF10[88]. In nitrofen-treated rats, expression of miR-200b in mesenchymal tissue is reduced. In addition, the distal-to-proximal gradient is diminished, with distal parabronchial cells being negative for miR-200b. Coleman *et al*. have shown that mice treated with nitrofen have increased expression of α-smooth muscle actin (α-SMA)[66]. This finding suggests that nitrofen accelerates mesenchymal differentiation into airway smooth muscle, associated with decreased expression of miR-200b.

In the late pseudoglandular stage (E15), the lungs separate from the surrounding splanchnic mesoderm as distinct organs inside the pleural cavity. Much of the lung mesenchyme remains positive for miR-200b, except for the proximal parabronchial tissue. Distal parabronchial cells, which are less differentiated progenitors, are positive for miR-200b in control rats and negative in nitrofen-treated rats (Figure 9).

As lung development advances into the canalicular stage, the population of differentiated fibroblasts increases and concurrently expression of miR-200b is reduced (Figure 12). In parabronchial cells, expression of miR-200b is restricted to distal bronchioles near the elongating tips. In CDH rats, the mesenchymal layer appears thickened with markedly reduced miR-200b expression. Specialized mesenchymal cells with epithelial features, including the mesothelium and endothelium, express miR-200b (Figure 13). Mesothelial cells, which line the pleural cavity, are strongly positive for miR-200b expression. In CDH rats, endothelial cells are less likely to stain positive. Whether this contributes to the pathogenesis of PPHN in nitrofen-induced CDH remains to be determined. In this study endothelial cells were identified based on histologic appearance of lining the inside of blood vessels. Confirmation of the role of miR-200b in endothelial differentiation requires further study including combined ISH and IHC using specific markers for endothelial cells. Another possible mechanism for PPHN in nitrofen-induced CDH is increased muscular thickening through upregulation of α-SMA as suggested by Coleman *et al*.[66].

In the saccular stage, much of the lung mesenchyme has fully differentiated into fibroblasts and airway smooth muscle cells. These cells are devoid of miR-200b. Terminal sacs also contain a population of negative staining cells, which are much more numerous in nitrofen-induced CDH, particularly in the severe phenotype (Figure 15). The identity of these cells and whether they are of epithelial or mesenchymal origin is unknown. For example, these cells could represent abnormal proliferation of lipofibroblasts, which appear during the alveolar stage and play a role in the production of ECM and as accessory cells to type II pneumocytes[89].

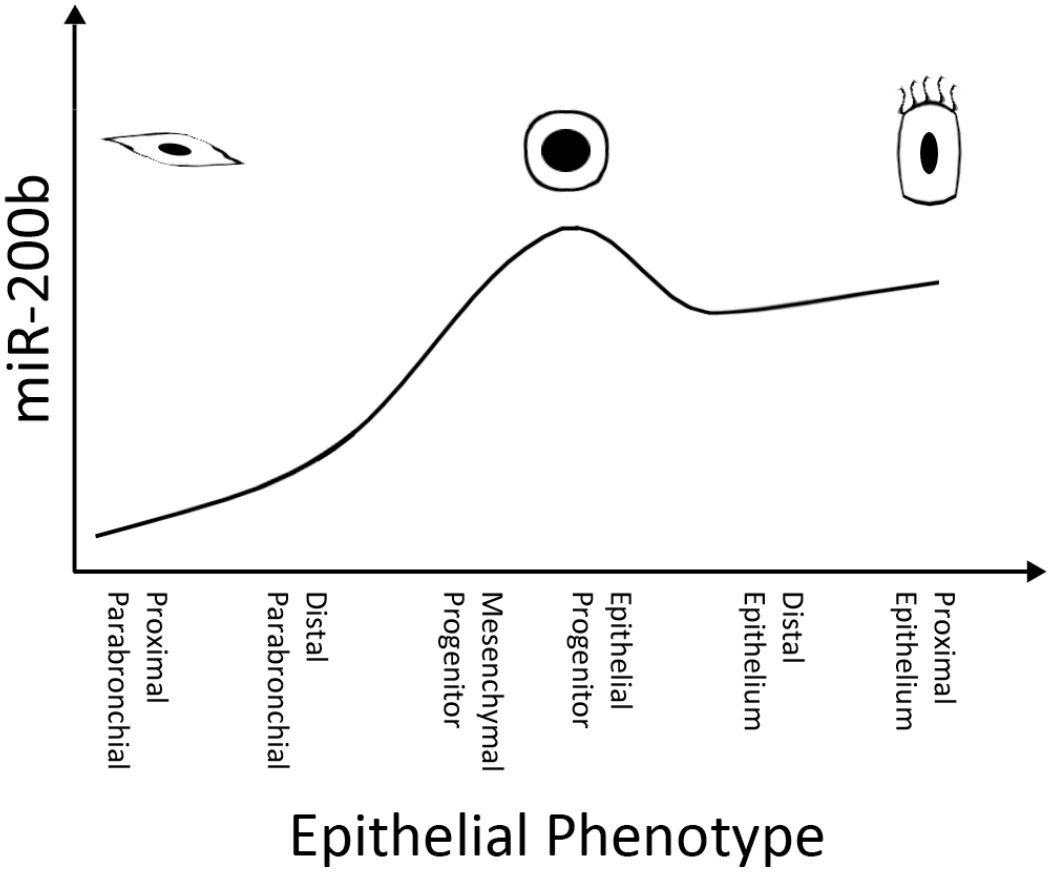

Figure 20. Expression of miR-200b favors an epithelial phenotype – In mesenchymal tissue, miR-200b expression decreases with increasing differentiation into parabronchial smooth muscle. In epithelial tissue, miR-200b expression is highest at the elongating tips (epithelial progenitors) and remains high during differentiation into proximal epithelium.

4.2. miR-200b & Epithelial Differentiation

In early lung development (pseudoglandular to canalicular stage) expression of miR-200b is highest at the tips of the elongating bronchial tree. These structures are quite prominent in ISH staining and their location was confirmed through serial sectioning (Figure 7). Interestingly they are more numerous in control lungs compared to CDH lungs, particularly at E18 (Figure 12). This is expected, since hypoplastic lungs have fewer

elongating tips per square area of lung due to reduced bronchial branching. Recently, Rawlins *et al*. have shown that distal tip cells are epithelial progenitors that give rise to the more differentiated proximal cells[90]. Unlike mesenchymal tissue, miR-200b expression continues in proximal epithelium.

In the saccular stage, proximal epithelial cells have higher expression of miR-200b compared to the more distal alveolar cells (Figure 15). In addition, tip structures are distinctly absent. This is an expected finding, since bronchial branching has ceased by the saccular stage.

4.3. Role of EMT/MET in Lung Development

This is the first study to suggest a role for EMT/MET in embryonic lung development. Evidence for this phenomenon comes from IHC experiments showing expression of vimentin, typically a mesenchymal marker, in distal epithelium throughout the pseudoglandular and canalicular stages (Figures 18 and 19). Initially this finding was surprising, because distal epithelium also expresses high levels of miR-200b, which normally inhibits expression of vimentin through downregulation of TGF-β/SMAD signaling. Explanation for this paradox came from concurrent studies of interactions between miR-200b and TGF-β in cultures of bronchial epithelial cells (unpublished data). Mimics of miR-200b decreased TGF-β/SMAD signaling, while nitrofen and inhibitors of miR-200b increased it. On the other hand, exogenous TGF-β resulted in a multifold increase in expression of miR-200b, while nitrofen decreased miR-200b expression. Taken together, these results indicate that miR-200b functions as a regulator of TGF-β/SMAD signaling through a negative feedback loop. In addition nitrofen decreases miR-200b levels independent of TGF-β (Figure 21).

Based on these observations we have proposed a working model for the role of miR-200b in early lung development (Figure 21). In the pseudoglandular and canalicular stages, distal epithelial progenitor cells have mesenchymal features that allow them to be invasive and grow into the surrounding tissue. This is an example of epithelial-to-mesenchymal transition. This phenotype is imparted upon them by growth factors, such as FGF10 that are released by mesenchymal progenitor cells. FGF10 is essential for induction of EMT during myocardial development[91]. During lung branching morphogenesis, BMP4, a member of the TGF-β superfamily, is expressed in high amounts in distal epithelium in response to FGF10[37]. In addition to facilitating elongation, epithelial progenitor cells must also differentiate into more proximal epithelial tissue. This process is an example of mesenchymal-to-epithelial transition and is initiated by miR-200b through a negative feedback mechanism.

Support for this hypothesis comes from the pattern of staining for vimentin in IHC slides. Vimentin is expressed in high amounts distally and drops gradually in more proximal epithelium (Figure 18). There is likely a delay between activation of miR-200b and its effect on downstream targets such as vimentin through production and inhibition of various transcription factors. This delay would be essential to allow epithelial growth before the process of differentiation takes over. MET might also occur in other aspects of lung development. As mentioned above endothelial and mesothelial cells, which are of mesenchymal origin, express miR-200b (Figure 13). Interestingly these cell types have epithelial features, such as lining tubular structures or forming sheets.

There is accumulating evidence that EMT is not conversion of epithelial cells into fibroblasts, but rather conversion of differentiated epithelial cells into less differentiated

progenitor or stem cells with mesenchymal features (see review by Thiery *et al.*[73]). What distinguished EMT during development from EMT in carcinogenesis is the presence of a robust regulatory system mediated at least partly through action of miRNA. Indeed, many aggressive cancers have reduced expression of members of the miR-200 family, which allows them to escape this regulatory mechanism[92-94]. Given its effects on miR-200b, it is not surprising that nitrofen is a carcinogen in adult rats[95].

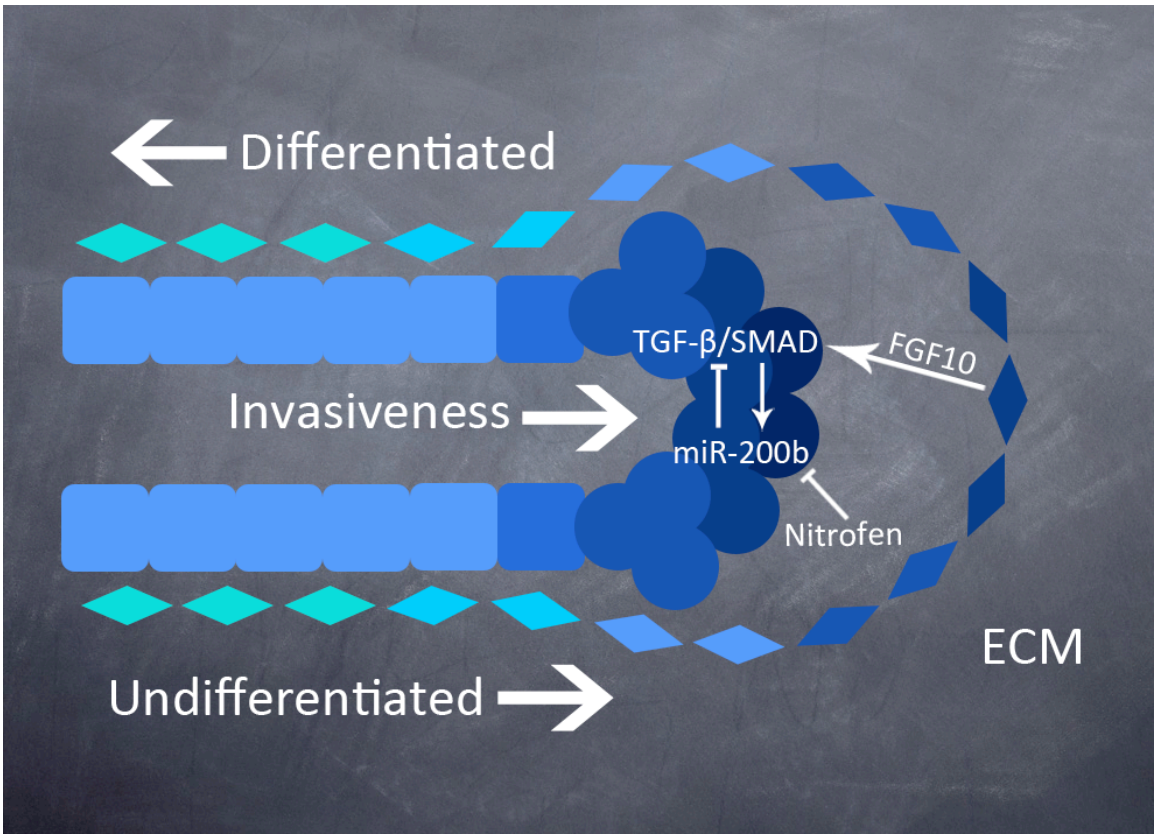

Figure 21. Role of miR-200b in early lung development (blue to green denotes transition from high to low miR-200b expression) – Distal mesenchymal progenitor cells induce epithelial proliferation and migration through FGF10-induced activation of TGF-β/SMAD signaling. miR-200b facilitates epithelial differentiation through a negative feedback loop. Nitrofen delays epithelial differentiation through inhibition of miR-200b.

4.4. Human vs. Nitrofen-induced CDH

Increased expression of TGF-β1 and TβRI in nitrofen-induced CDH has previously been demonstrated using IHC and real-time quantitative polymerase chain reaction (qPCR)[96, 97]. There are two possible mechanisms for lung hypoplasia in this context. First, accelerated mesenchymal differentiation would decrease the pool of progenitor mesenchymal cells that are required for FGF-10 production. Ramasamy *et al*. have shown that FGF10 dosage is critical for amplification of epithelial progenitor cells[98]. Second, fibroblast differentiation can lead to increased ECM production, hindering epithelial growth. In mice, overexpression of TGF-β1 results in lung hypoplasia characterized by decreased epithelial differentiation, thickened pulmonary mesenchyme and altered distribution of parabronchial α-SMA to more distal expression[99, 100]. According to this model the primary reason for lung hypoplasia in nitrofen-induced CDH is a defect in mesenchymal tissue, which has been shown in recombinant experiments using fibroblasts isolated from nitrofen-treated lungs[65].

In the saccular stage, ISH identified two groups of CDH lungs based on amount of miR-200b staining (Figures 15-17). The severe phenotype was associated with larger hernias and smaller lungs, although we did not formally measure lung-to-body weight ratio, as this was an unexpected finding. One possible explanation for this outcome is a dose-response effect. It is known that not all embryos in a litter are affected equally by nitrofen administration. For example, only 60% of embryos in our nitrofen group developed CDH. Embryos that end up with bigger hernias and smaller lungs likely receive a higher effective dose of nitrofen that lasts into the saccular stage affecting cellular differentiation. This results in abnormal proliferation of cells that are negative for

miR-200b. In the mild phenotype the effect of nitrofen, which is administered on E9, on epithelial differentiation has diminished by saccular stage (E21), resulting in an increased number of alveolar cells that are positive for miR-200b.

Human and animal models of CDH have been contrasted by the degree of epithelial differentiation. In rats, CDH lungs have reduced levels of disaturated phosphatidylcholine and increased concentration of glycogen, both indicators of biochemical immaturity[101, 102]. These lungs are also deficient in expression of surfactant protein A (SP-A)[103]. Nitrofen treatment has consistently been shown to reduce markers of epithelial differentiation, including decreased expression of thyroid transcription factor-1 (TTF-1), clara cell secretory protein-10 (CC-10), and SP-C[24, 104]. In mice, nitrofen is associated with delayed epithelial differentiation, including persistence of TTF-1 in the periphery and decreased SP-A expression[66].

In human CDH, surfactant levels are normal. Amniotic fluid phospholipid analyses in 18 prenatally diagnosed CDH cases were comparable to normal fetuses of the same gestational age[105]. Bronchoalveolar lavage fluid of infants with CDH revealed normal phospholipid composition and surfactant synthesis and kinetics[106, 107]. Boucherat *et al*. found no difference in surfactant expression in 16 human lungs with CDH compared to age-matched controls. The lungs were also similar with respect to mediators of lung maturity, including TTF-1, and surfactant production[108]. Consistent with these findings, surfactant therapy has been shown to be of no benefit in term and preterm infants with CDH and may in fact be harmful[109, 110].

Using ISH we have shown that unlike nitrofen-induced CDH, human lungs contain an abundance of miR-200b-positive cells in terminal saccules and alveoli. This

finding accounts for normal epithelial differentiation in human CDH as opposed to nitrofen-treated rats. At this point we can only speculate on how increased miR-200b expression can lead to pulmonary hypoplasia. One possible mechanism in early lung development is reduced epithelial invasion through inhibition of TGF-β-induced EMT (Figure 21). Accelerated epithelial differentiation would reduce the time available for branching morphogenesis. This would result in small lungs that are biochemically mature. In addition, decreased TGF-β signaling might specifically affect late lung development during alveolarization. Chen *et al*. have shown that abrogation of TβRII in lung epithelium reduces alveolar septation. Interestingly, blockade of TβRII in mesenchymal tissue was associated with multiple musculoskeletal defects including CDH[111]. Similar to FGF10, TGF-β expression is highly regulated during lung development. This has led to the "Goldilocks" hypothesis, which states that TGF-β signaling has to be just right for normal development to occur[112]. In other words, both increased and decreased TGF-β signaling can lead to lung hypoplasia and this likely occurs due to differential effects of TGF-β in epithelial and mesenchymal tissue.

4.5. Other Predicted Target Genes for miR-200b

Regression methods predict hundreds of gene targets for miR-200b based on complementarity between the mature sequence of miRNA and the 3' UTR of mRNAs (for a complete list, see www.microRNA.org). As discussed previously, the reciprocal relationship between miR-200b and members of TGF-β/SMAD signaling has been established through *in vivo* studies and *in vitro* assays. While experimental evidence is lacking for most other predicted targets, several genes might be of interest due to their putative roles in lung development.

Fibronectin (FN) is an extracellular matrix protein that facilitates cellular binding to components of ECM. FN is expressed in response to *Wnt* signaling in distal epithelium and contributes to lung bud splitting at epithelial branch points[113]. Treating lung explants with anti-FN antibody or small interfering RNA (siRNA) inhibits branching morphogenesis, while FN supplementation promotes lung branching[113, 114]. FN contributes to lung bud splitting by enhancing interactions between cell membrane integrins and components of the basement membrane[114]. The 3' UTR of *FN1* has several binding sites for miR-200b. Therefore, changes in miR-200b expression might affect lung branching morphogenesis by perturbing *FN1* function.

Another potential target for miR-200b is neuregulin 1 (NRG1). This protein is a member of the neuregulin family, which plays a critical role in the development of the heart and the nervous system[115]. Neuregulins affect cellular proliferation and differentiation of neighboring cells by binding to the ERBB family of tyrosine kinase receptors. During the alveolar stage of lung development, NRG1 is expressed by lung fibroblasts and binds to ERBB receptors on type II epithelial cells to affect cellular proliferation and surfactant synthesis[116]. An association between miR-200b and NRG1 might explain the observed differences in surfactant synthesis between the human and animal models of CDH. Furthermore, it might account for the associated cardiac and nervous system anomalies in CDH.

4.6. Limitations & Future Directions

This is the first study to identify abnormal miRNA expression in human congenital disease. Given the difficulty of obtaining human tissues to study CDH, our results are limited by a small sample size.

We quantified in situ hybridization staining using a colocalization algorithm, which measures the area of staining without considering its intensity. This method is comparable to counting the number of positive-staining cells and is different from fluorescent-based analysis that includes an endogenous control for standardization of signal intensity. Currently our laboratory is using qPCR to measure fold differences in miR-200b expression between hypoplastic and control lungs.

How does nitrofen decease miR-200b expression? A possible mechanism might involve abnormal DNA methylation. The Madin Darby canine kidney (MDCK) cell line has been used extensively as an in vitro model of EMT, due to its propensity to undergo EMT in response to TGF-β. MDCK cells have all the hallmarks of epithelial cells; however upon treatment with TGF-β they acquire mesenchymal features and even begin to produce TGF-β in an autocrine fashion. In these cells, prolonged exposure to TGF-β promotes DNA methylation of the miR-200 family promoters[117]. Abnormal methylation of the miR-200b promoter can disrupt its negative feedback relationship with TGF-β, resulting in continued activation of TGF-β/SMAD signaling. In the future we plan to study DNA methylation in the nitrofen model using a readily available PCR assay[118].

REFERENCES

1. Stege, G., Fenton, A. & Jaffray, B. Nihilism in the 1990s: the true mortality of congenital diaphragmatic hernia. *Pediatrics* **112**, 532-535 (2003).

2. Colvin, J., Bower, C., Dickinson, J. E. & Sokol, J. Outcomes of congenital diaphragmatic hernia: a population-based study in Western Australia. *Pediatrics* **116**, e356-63 (2005).

3. Ladd, W. E. & Gross, R. E. Congenital Diaphragmatic Hernia. *N. Engl. J. Med.* **223**, 917-925 (1940).

4. Kays, D. W., Langham, M. R.,Jr, Ledbetter, D. J. & Talbert, J. L. Detrimental effects of standard medical therapy in congenital diaphragmatic hernia. *Ann. Surg.* **230**, 340-8; discussion 348-51 (1999).

5. Geggel, R. L., Murphy, J. D., Langleben, D., Crone, R. K., Vacanti, J. P. & Reid, L. M. Congenital diaphragmatic hernia: arterial structural changes and persistent pulmonary hypertension after surgical repair. *J. Pediatr.* **107**, 457-464 (1985).

6. Sakai, H., Tamura, M., Hosokawa, Y., Bryan, A. C., Barker, G. A. & Bohn, D. J. Effect of surgical repair on respiratory mechanics in congenital diaphragmatic hernia. *J. Pediatr.* **111**, 432-438 (1987).

7. Harting, M. T. & Lally, K. P. Surgical management of neonates with congenital diaphragmatic hernia. *Semin. Pediatr. Surg.* **16**, 109-114 (2007).

8. Javid, P. J., Jaksic, T., Skarsgard, E. D., Lee, S. & Canadian Neonatal Network. Survival rate in congenital diaphragmatic hernia: the experience of the Canadian Neonatal Network. *J. Pediatr. Surg.* **39**, 657-660 (2004).

9. Nasr, A., Langer, J. C. & Canadian Pediatric Surgery Network. Influence of location of delivery on outcome in neonates with congenital diaphragmatic hernia. *J. Pediatr. Surg.* **46**, 814-816 (2011).

10. Drummond, W. H., Gregory, G. A., Heymann, M. A. & Phibbs, R. A. The independent effects of hyperventilation, tolazoline, and dopamine on infants with persistent pulmonary hypertension. *J. Pediatr.* **98**, 603-611 (1981).

11. Reynolds, M., Luck, S. R. & Lappen, R. The "critical" neonate with diaphragmatic hernia: a 21-year perspective. *J. Pediatr. Surg.* **19**, 364-369 (1984).

12. Wung, J. T., James, L. S., Kilchevsky, E. & James, E. Management of infants with severe respiratory failure and persistence of the fetal circulation, without hyperventilation. *Pediatrics* **76**, 488-494 (1985).

13. Wung, J. T., Sahni, R., Moffitt, S. T., Lipsitz, E. & Stolar, C. J. Congenital diaphragmatic hernia: survival treated with very delayed surgery, spontaneous respiration, and no chest tube. *J. Pediatr. Surg.* **30**, 406-409 (1995).

14. Frenckner, B., Ehren, H., Granholm, T., Linden, V. & Palmer, K. Improved results in patients who have congenital diaphragmatic hernia using preoperative stabilization, extracorporeal membrane oxygenation, and delayed surgery. *J. Pediatr. Surg.* **32**, 1185-1189 (1997).

15. Seetharamaiah, R., Younger, J. G., Bartlett, R. H., Hirschl, R. B. & Congenital Diaphragmatic Hernia Study Group. Factors associated with survival in infants with congenital diaphragmatic hernia requiring extracorporeal membrane oxygenation: a report from the Congenital Diaphragmatic Hernia Study Group. *J. Pediatr. Surg.* **44**, 1315-1321 (2009).

16. Guner, Y. S., Khemani, R. G., Qureshi, F. G., Wee, C. P., Austin, M. T., Dorey, F., Rycus, P. T., Ford, H. R., Friedlich, P. & Stein, J. E. Outcome analysis of neonates with congenital diaphragmatic hernia treated with venovenous vs venoarterial extracorporeal membrane oxygenation. *J. Pediatr. Surg.* **44**, 1691-1701 (2009).

17. Davis, P. J., Firmin, R. K., Manktelow, B., Goldman, A. P., Davis, C. F., Smith, J. H., Cassidy, J. V. & Shekerdemian, L. S. Long-term outcome following extracorporeal membrane oxygenation for congenital diaphragmatic hernia: the UK experience. *J. Pediatr.* **144**, 309-315 (2004).

18. Harrison, M. R., Adzick, N. S., Longaker, M. T., Goldberg, J. D., Rosen, M. A., Filly, R. A., Evans, M. I. & Golbus, M. S. Successful Repair in Utero of a Fetal Diaphragmatic Hernia after Removal of Herniated Viscera from the Left Thorax. *N. Engl. J. Med.* **322**, 1582-1584 (1990).

19. Harrison, M. R., Mychaliska, G. B., Albanese, C. T., Jennings, R. W., Farrell, J. A., Hawgood, S., Sandberg, P., Levine, A. H., Lobo, E. & Filly, R. A. Correction of congenital diaphragmatic hernia in utero IX: fetuses with poor prognosis (liver herniation and low lung-to-head ratio) can be saved by fetoscopic temporary tracheal occlusion. *J. Pediatr. Surg.* **33**, 1017-22; discussion 1022-3 (1998).

20. Harrison, M. R., Keller, R. L., Hawgood, S. B., Kitterman, J. A., Sandberg, P. L., Farmer, D. L., Lee, H., Filly, R. A., Farrell, J. A. & Albanese, C. T. A Randomized Trial of Fetal Endoscopic Tracheal Occlusion for Severe Fetal Congenital Diaphragmatic Hernia. *N. Engl. J. Med.* **349**, 1916-1924 (2003).

21. Larson, J. E. & Cohen, J. C. Improvement of pulmonary hypoplasia associated with congenital diaphragmatic hernia by in utero CFTR gene therapy. *Am. J. Physiol. Lung Cell. Mol. Physiol.* **291**, L4-10 (2006).

22. Lally, K. P., Lally, P. A., Van Meurs, K. P., Bohn, D. J., Davis, C. F., Rodgers, B., Bhatia, J., Dudell, G. & Congenital Diaphragmatic Hernia Study Group. Treatment evolution in high-risk congenital diaphragmatic hernia: ten years' experience with diaphragmatic agenesis. *Ann. Surg.* **244**, 505-513 (2006).

23. van Loenhout, R. B., Tibboel, D., Post, M. & Keijzer, R. Congenital diaphragmatic hernia: comparison of animal models and relevance to the human situation. *Neonatology* **96**, 137-149 (2009).

24. Keijzer, R., Liu, J., Deimling, J., Tibboel, D. & Post, M. Dual-hit hypothesis explains pulmonary hypoplasia in the nitrofen model of congenital diaphragmatic hernia. *Am. J. Pathol.* **156**, 1299-1306 (2000).

25. Alessandri, L., Brayer, C., Attali, T., Samperiz, S., Tiran-Rajaofera, I., Ramful, D. & Pilorget, H. Fryns syndrome without diaphragmatic hernia. Report on a new case and review of the literature. *Genet. Couns.* **16**, 363-370 (2005).

26. Finer, N. N. & Barrington, K. J. Nitric oxide for respiratory failure in infants born at or near term. *Cochrane Database Syst. Rev.* **(4)**, CD000399 (2006).

27. Neonatal Inhaled Nitric Oxide Study Group (NINOS). Inhaled nitric oxide and hypoxic respiratory failure in infants with congenital diaphragmatic hernia. *Pediatrics* **99**, 838-845 (1997).

28. Thebaud, B., Petit, T., De Lagausie, P., Dall'Ava-Santucci, J., Mercier, J. C. & Dinh-Xuan, A. T. Altered guanylyl-cyclase activity in vitro of pulmonary arteries from fetal

lambs with congenital diaphragmatic hernia. *Am. J. Respir. Cell Mol. Biol.* **27**, 42-47 (2002).

29. de Buys Roessingh, A., Fouquet, V., Aigrain, Y., Mercier, J. C., de Lagausie, P. & Dinh-Xuan, A. T. Nitric oxide activity through guanylate cyclase and phosphodiesterase modulation is impaired in fetal lambs with congenital diaphragmatic hernia. *J. Pediatr. Surg.* **46**, 1516-1522 (2011).

30. Keijzer, R. & Puri, P. Congenital diaphragmatic hernia. *Semin. Pediatr. Surg.* **19**, 180-185 (2010).

31. Greer, J. J., Cote, D., Allan, D. W., Zhang, W., Babiuk, R. P., Ly, L., Lemke, R. P. & Bagnall, K. Structure of the primordial diaphragm and defects associated with nitrofen-induced CDH. *J. Appl. Physiol.* **89**, 2123-2129 (2000).

32. Babiuk, R. P., Zhang, W., Clugston, R., Allan, D. W. & Greer, J. J. Embryological origins and development of the rat diaphragm. *J. Comp. Neurol.* **455**, 477-487 (2003).

33. Metzger, R. J., Klein, O. D., Martin, G. R. & Krasnow, M. A. The branching programme of mouse lung development. *Nature* **453**, 745-750 (2008).

34. Warburton, D., El-Hashash, A., Carraro, G., Tiozzo, C., Sala, F., Rogers, O., De Langhe, S., Kemp, P. J., Riccardi, D., Torday, J., Bellusci, S., Shi, W., Lubkin, S. R. & Jesudason, E. Lung organogenesis. *Curr. Top. Dev. Biol.* **90**, 73-158 (2010).

35. Urase, K., Mukasa, T., Igarashi, H., Ishii, Y., Yasugi, S., Momoi, M. Y. & Momoi, T. Spatial expression of Sonic hedgehog in the lung epithelium during branching morphogenesis. *Biochem. Biophys. Res. Commun.* **225**, 161-166 (1996).

36. Bellusci, S., Furuta, Y., Rush, M. G., Henderson, R., Winnier, G. & Hogan, B. L. Involvement of Sonic hedgehog (Shh) in mouse embryonic lung growth and morphogenesis. *Development* **124**, 53-63 (1997).

37. Weaver, M., Dunn, N. R. & Hogan, B. L. Bmp4 and Fgf10 play opposing roles during lung bud morphogenesis. *Development* **127**, 2695-2704 (2000).

38. Min, H., Danilenko, D. M., Scully, S. A., Bolon, B., Ring, B. D., Tarpley, J. E., DeRose, M. & Simonet, W. S. Fgf-10 is required for both limb and lung development and exhibits striking functional similarity to Drosophila branchless. *Genes Dev.* **12**, 3156-3161 (1998).

39. Bragg, A. D., Moses, H. L. & Serra, R. Signaling to the epithelium is not sufficient to mediate all of the effects of transforming growth factor beta and bone morphogenetic protein 4 on murine embryonic lung development. *Mech. Dev.* **109**, 13-26 (2001).

40. Eblaghie, M. C., Reedy, M., Oliver, T., Mishina, Y. & Hogan, B. L. Evidence that autocrine signaling through Bmpr1a regulates the proliferation, survival and morphogenetic behavior of distal lung epithelial cells. *Dev. Biol.* **291**, 67-82 (2006).

41. Fauza, D. O. & Wilson, J. M. Congenital diaphragmatic hernia and associated anomalies: Their incidence, identification, and impact on prognosis. *J. Pediatr. Surg.* **29**, 1113-1117 (1994).

42. Wilson, J. G., Roth, C. B. & Warkany, J. An analysis of the syndrome of malformations induced by maternal vitamin A deficiency. Effects of restoration of vitamin A at various times during gestation. *Am. J. Anat.* **92**, 189-217 (1953).

43. Thebaud, B., Tibboel, D., Rambaud, C., Mercier, J. C., Bourbon, J. R., Dinh-Xuan, A. T. & Archer, S. L. Vitamin A decreases the incidence and severity of nitrofen-induced congenital diaphragmatic hernia in rats. *Am. J. Physiol.* **277**, L423-9 (1999).

44. Dickman, E. D., Thaller, C. & Smith, S. M. Temporally-regulated retinoic acid depletion produces specific neural crest, ocular and nervous system defects. *Development* **124**, 3111-3121 (1997).

45. Beurskens, L. W., Tibboel, D., Lindemans, J., Duvekot, J. J., Cohen-Overbeek, T. E., Veenma, D. C., de Klein, A., Greer, J. J. & Steegers-Theunissen, R. P. Retinol status of newborn infants is associated with congenital diaphragmatic hernia. *Pediatrics* **126**, 712-720 (2010).

46. Laurent, L., Wong, E., Li, G., Huynh, T., Tsirigos, A., Ong, C. T., Low, H. M., Kin Sung, K. W., Rigoutsos, I., Loring, J. & Wei, C. L. Dynamic changes in the human methylome during differentiation. *Genome Res.* **20**, 320-331 (2010).

47. Zhao, Y., Ransom, J. F., Li, A., Vedantham, V., von Drehle, M., Muth, A. N., Tsuchihashi, T., McManus, M. T., Schwartz, R. J. & Srivastava, D. Dysregulation of cardiogenesis, cardiac conduction, and cell cycle in mice lacking miRNA-1-2. *Cell* **129**, 303-317 (2007).

48. Rodriguez, A., Griffiths-Jones, S., Ashurst, J. L. & Bradley, A. Identification of mammalian microRNA host genes and transcription units. *Genome Res.* **14**, 1902-1910 (2004).

49. Cai, X., Hagedorn, C. H. & Cullen, B. R. Human microRNAs are processed from capped, polyadenylated transcripts that can also function as mRNAs. *RNA* **10**, 1957-1966 (2004).

50. Lee, Y., Ahn, C., Han, J., Choi, H., Kim, J., Yim, J., Lee, J., Provost, P., Radmark, O., Kim, S. & Kim, V. N. The nuclear RNase III Drosha initiates microRNA processing. *Nature* **425**, 415-419 (2003).

51. Han, J., Lee, Y., Yeom, K. H., Nam, J. W., Heo, I., Rhee, J. K., Sohn, S. Y., Cho, Y., Zhang, B. T. & Kim, V. N. Molecular basis for the recognition of primary microRNAs by the Drosha-DGCR8 complex. *Cell* **125**, 887-901 (2006).

52. Ambros, V. The functions of animal microRNAs. *Nature* **431**, 350-355 (2004).

53. Iwasaki, S., Kawamata, T. & Tomari, Y. Drosophila argonaute1 and argonaute2 employ distinct mechanisms for translational repression. *Mol. Cell* **34**, 58-67 (2009).

54. Mathonnet, G., Fabian, M. R., Svitkin, Y. V., Parsyan, A., Huck, L., Murata, T., Biffo, S., Merrick, W. C., Darzynkiewicz, E., Pillai, R. S., Filipowicz, W., Duchaine, T. F. & Sonenberg, N. MicroRNA inhibition of translation initiation in vitro by targeting the cap-binding complex eIF4F. *Science* **317**, 1764-1767 (2007).

55. Harris, K. S., Zhang, Z., McManus, M. T., Harfe, B. D. & Sun, X. Dicer function is essential for lung epithelium morphogenesis. *Proc. Natl. Acad. Sci. U. S. A.* **103**, 2208-2213 (2006).

56. Lu, J., Qian, J., Chen, F., Tang, X., Li, C. & Cardoso, W. V. Differential expression of components of the microRNA machinery during mouse organogenesis. *Biochem. Biophys. Res. Commun.* **334**, 319-323 (2005).

57. Dong, J., Jiang, G., Asmann, Y. W., Tomaszek, S., Jen, J., Kislinger, T. & Wigle, D. A. MicroRNA networks in mouse lung organogenesis. *PLoS One* **5**, e10854 (2010).

58. Hayashita, Y., Osada, H., Tatematsu, Y., Yamada, H., Yanagisawa, K., Tomida, S., Yatabe, Y., Kawahara, K., Sekido, Y. & Takahashi, T. A polycistronic microRNA

cluster, miR-17-92, is overexpressed in human lung cancers and enhances cell proliferation. *Cancer Res.* **65**, 9628-9632 (2005).

59. Lu, Y., Thomson, J. M., Wong, H. Y., Hammond, S. M. & Hogan, B. L. Transgenic over-expression of the microRNA miR-17-92 cluster promotes proliferation and inhibits differentiation of lung epithelial progenitor cells. *Dev. Biol.* **310**, 442-453 (2007).

60. Ventura, A., Young, A. G., Winslow, M. M., Lintault, L., Meissner, A., Erkeland, S. J., Newman, J., Bronson, R. T., Crowley, D., Stone, J. R., Jaenisch, R., Sharp, P. A. & Jacks, T. Targeted deletion reveals essential and overlapping functions of the miR-17 through 92 family of miRNA clusters. *Cell* **132**, 875-886 (2008).

61. Yanaihara, N., Caplen, N., Bowman, E., Seike, M., Kumamoto, K., Yi, M., Stephens, R. M., Okamoto, A., Yokota, J., Tanaka, T., Calin, G. A., Liu, C. G., Croce, C. M. & Harris, C. C. Unique microRNA molecular profiles in lung cancer diagnosis and prognosis. *Cancer. Cell.* **9**, 189-198 (2006).

62. Navarro, A., Marrades, R. M., Vinolas, N., Quera, A., Agusti, C., Huerta, A., Ramirez, J., Torres, A. & Monzo, M. MicroRNAs expressed during lung cancer development are expressed in human pseudoglandular lung embryogenesis. *Oncology* **76**, 162-169 (2009).

63. Johnson, S. M., Grosshans, H., Shingara, J., Byrom, M., Jarvis, R., Cheng, A., Labourier, E., Reinert, K. L., Brown, D. & Slack, F. J. RAS is regulated by the let-7 microRNA family. *Cell* **120**, 635-647 (2005).

64. Lu, Y., Okubo, T., Rawlins, E. & Hogan, B. L. Epithelial progenitor cells of the embryonic lung and the role of microRNAs in their proliferation. *Proc. Am. Thorac. Soc.* **5**, 300-304 (2008).

65. van Loenhout, R. B., Tseu, I., Fox, E. K., Huang, Z., Tibboel, D., Post, M. & Keijzer, R. The pulmonary mesenchymal tissue layer is defective in an in vitro recombinant model of nitrofen-induced lung hypoplasia. *Am. J. Pathol.* **180**, 48-60 (2012).

66. Coleman, C., Zhao, J., Gupta, M., Buckley, S., Tefft, J. D., Wuenschell, C. W., Minoo, P., Anderson, K. D. & Warburton, D. Inhibition of vascular and epithelial differentiation in murine nitrofen-induced diaphragmatic hernia. *Am. J. Physiol.* **274**, L636-46 (1998).

67. Leptin, M. Gastrulation movements: the logic and the nuts and bolts. *Dev. Cell.* **8**, 305-320 (2005).

68. Sauka-Spengler, T. & Bronner-Fraser, M. A gene regulatory network orchestrates neural crest formation. *Nat. Rev. Mol. Cell Biol.* **9**, 557-568 (2008).

69. Carroll, T. J., Park, J. S., Hayashi, S., Majumdar, A. & McMahon, A. P. Wnt9b plays a central role in the regulation of mesenchymal to epithelial transitions underlying organogenesis of the mammalian urogenital system. *Dev. Cell.* **9**, 283-292 (2005).

70. Stark, K., Vainio, S., Vassileva, G. & McMahon, A. P. Epithelial transformation of metanephric mesenchyme in the developing kidney regulated by Wnt-4. *Nature* **372**, 679-683 (1994).

71. Mercado-Pimentel, M. E. & Runyan, R. B. Multiple transforming growth factor-beta isoforms and receptors function during epithelial-mesenchymal cell transformation in the embryonic heart. *Cells Tissues Organs* **185**, 146-156 (2007).

72. Nakajima, Y., Yamagishi, T., Hokari, S. & Nakamura, H. Mechanisms involved in valvuloseptal endocardial cushion formation in early cardiogenesis: roles of transforming

growth factor (TGF)-beta and bone morphogenetic protein (BMP). *Anat. Rec.* **258**, 119-127 (2000).

73. Polyak, K. & Weinberg, R. A. Transitions between epithelial and mesenchymal states: acquisition of malignant and stem cell traits. *Nat. Rev. Cancer.* **9**, 265-273 (2009).

74. Kim, K. K., Kugler, M. C., Wolters, P. J., Robillard, L., Galvez, M. G., Brumwell, A. N., Sheppard, D. & Chapman, H. A. Alveolar epithelial cell mesenchymal transition develops in vivo during pulmonary fibrosis and is regulated by the extracellular matrix. *Proc. Natl. Acad. Sci. U. S. A.* **103**, 13180-13185 (2006).

75. Iwano, M., Plieth, D., Danoff, T. M., Xue, C., Okada, H. & Neilson, E. G. Evidence that fibroblasts derive from epithelium during tissue fibrosis. *J. Clin. Invest.* **110**, 341-350 (2002).

76. Rastaldi, M. P., Ferrario, F., Giardino, L., Dell'Antonio, G., Grillo, C., Grillo, P., Strutz, F., Muller, G. A., Colasanti, G. & D'Amico, G. Epithelial-mesenchymal transition of tubular epithelial cells in human renal biopsies. *Kidney Int.* **62**, 137-146 (2002).

77. Xu, J., Lamouille, S. & Derynck, R. TGF-beta-induced epithelial to mesenchymal transition. *Cell Res.* **19**, 156-172 (2009).

78. Brabletz, S. & Brabletz, T. The ZEB/miR-200 feedback loop--a motor of cellular plasticity in development and cancer? *EMBO Rep.* **11**, 670-677 (2010).

79. Kato, M., Arce, L., Wang, M., Putta, S., Lanting, L. & Natarajan, R. A microRNA circuit mediates transforming growth factor-beta1 autoregulation in renal glomerular mesangial cells. *Kidney Int.* **80**, 358-368 (2011).

80. Burk, U., Schubert, J., Wellner, U., Schmalhofer, O., Vincan, E., Spaderna, S. & Brabletz, T. A reciprocal repression between ZEB1 and members of the miR-200 family promotes EMT and invasion in cancer cells. *EMBO Rep.* **9**, 582-589 (2008).

81. Liu, Y., El-Naggar, S., Darling, D. S., Higashi, Y. & Dean, D. C. Zeb1 links epithelial-mesenchymal transition and cellular senescence. *Development* **135**, 579-588 (2008).

82. Gregory, P. A., Bert, A. G., Paterson, E. L., Barry, S. C., Tsykin, A., Farshid, G., Vadas, M. A., Khew-Goodall, Y. & Goodall, G. J. The miR-200 family and miR-205 regulate epithelial to mesenchymal transition by targeting ZEB1 and SIP1. *Nat. Cell Biol.* **10**, 593-601 (2008).

83. Yang, S., Banerjee, S., de Freitas, A., Sanders, Y. Y., Ding, Q., Matalon, S., Thannickal, V. J., Abraham, E. & Liu, G. Participation of miR-200 in pulmonary fibrosis. *Am. J. Pathol.* **180**, 484-493 (2012).

84. Jorgensen, S., Baker, A., Moller, S. & Nielsen, B. S. Robust one-day in situ hybridization protocol for detection of microRNAs in paraffin samples using LNA probes. *Methods* **52**, 375-381 (2010).

85. Sempere, L. F., Preis, M., Yezefski, T., Ouyang, H., Suriawinata, A. A., Silahtaroglu, A., Conejo-Garcia, J. R., Kauppinen, S., Wells, W. & Korc, M. Fluorescence-based codetection with protein markers reveals distinct cellular compartments for altered MicroRNA expression in solid tumors. *Clin. Cancer Res.* **16**, 4246-4255 (2010).

86. Chi, V. & Chandy, K. G. Immunohistochemistry: paraffin sections using the Vectastain ABC kit from vector labs. *J. Vis. Exp.* **(8)**, 308 (2007).

87. Krajewska, M., Smith, L. H., Rong, J., Huang, X., Hyer, M. L., Zeps, N., Iacopetta, B., Linke, S. P., Olson, A. H., Reed, J. C. & Krajewski, S. Image analysis algorithms for immunohistochemical assessment of cell death events and fibrosis in tissue sections. *J. Histochem. Cytochem.* **57**, 649-663 (2009).

88. Mailleux, A. A., Kelly, R., Veltmaat, J. M., De Langhe, S. P., Zaffran, S., Thiery, J. P. & Bellusci, S. Fgf10 expression identifies parabronchial smooth muscle cell progenitors and is required for their entry into the smooth muscle cell lineage. *Development* **132**, 2157-2166 (2005).

89. Schultz, C. J., Torres, E., Londos, C. & Torday, J. S. Role of adipocyte differentiation-related protein in surfactant phospholipid synthesis by type II cells. *Am. J. Physiol. Lung Cell. Mol. Physiol.* **283**, L288-96 (2002).

90. Rawlins, E. L., Clark, C. P., Xue, Y. & Hogan, B. L. The Id2+ distal tip lung epithelium contains individual multipotent embryonic progenitor cells. *Development* **136**, 3741-3745 (2009).

91. Vega-Hernandez, M., Kovacs, A., De Langhe, S. & Ornitz, D. M. FGF10/FGFR2b signaling is essential for cardiac fibroblast development and growth of the myocardium. *Development* **138**, 3331-3340 (2011).

92. Sun, L., Yao, Y., Liu, B., Lin, Z., Lin, L., Yang, M., Zhang, W., Chen, W., Pan, C., Liu, Q., Song, E. & Li, J. MiR-200b and miR-15b regulate chemotherapy-induced epithelial-mesenchymal transition in human tongue cancer cells by targeting BMI1. *Oncogene* **31**, 432-445 (2012).

93. Baffa, R., Fassan, M., Volinia, S., O'Hara, B., Liu, C. G., Palazzo, J. P., Gardiman, M., Rugge, M., Gomella, L. G., Croce, C. M. & Rosenberg, A. MicroRNA expression

profiling of human metastatic cancers identifies cancer gene targets. *J. Pathol.* **219**, 214-221 (2009).

94. Braun, J., Hoang-Vu, C., Dralle, H. & Huttelmaier, S. Downregulation of microRNAs directs the EMT and invasive potential of anaplastic thyroid carcinomas. *Oncogene* **29**, 4237-4244 (2010).

95. National Toxicology Program. Bioassay of nitrofen for possible carcinogenicity. *Natl. Cancer. Inst. Carcinog. Tech. Rep. Ser.* **26**, 1-87 (1978).

96. Chen, G., Qiao, Y., Xiao, X., Zheng, S. & Chen, L. Effects of estrogen on lung development in a rat model of diaphragmatic hernia. *J. Pediatr. Surg.* **45**, 2340-2345 (2010).

97. Xu, C., Liu, W., Chen, Z., Wang, Y., Xiong, Z. & Ji, Y. Effect of prenatal tetrandrine administration on transforming growth factor-beta1 level in the lung of nitrofen-induced congenital diaphragmatic hernia rat model. *J. Pediatr. Surg.* **44**, 1611-1620 (2009).

98. Ramasamy, S. K., Mailleux, A. A., Gupte, V. V., Mata, F., Sala, F. G., Veltmaat, J. M., Del Moral, P. M., De Langhe, S., Parsa, S., Kelly, L. K., Kelly, R., Shia, W., Keshet, E., Minoo, P., Warburton, D. & Bellusci, S. Fgf10 dosage is critical for the amplification of epithelial cell progenitors and for the formation of multiple mesenchymal lineages during lung development. *Dev. Biol.* **307**, 237-247 (2007).

99. Zhou, L., Dey, C. R., Wert, S. E. & Whitsett, J. A. Arrested lung morphogenesis in transgenic mice bearing an SP-C-TGF-beta 1 chimeric gene. *Dev. Biol.* **175**, 227-238 (1996).

100. Zeng, X., Gray, M., Stahlman, M. T. & Whitsett, J. A. TGF-beta1 perturbs vascular development and inhibits epithelial differentiation in fetal lung in vivo. *Dev. Dyn.* **221**, 289-301 (2001).

101. Alfanso, L. F., Arnaiz, A., Alvarez, F. J., Qi, B., Diez-Pardo, J. A., Vallis-i-Soler, A. & Tovar, J. A. Lung hypoplasia and surfactant system immaturity induced in the fetal rat by prenatal exposure to nitrofen. *Biol. Neonate* **69**, 94-100 (1996).

102. Suen, H. C., Catlin, E. A., Ryan, D. P., Wain, J. C. & Donahoe, P. K. Biochemical immaturity of lungs in congenital diaphragmatic hernia. *J. Pediatr. Surg.* **28**, 471-5; discussion 476-7 (1993).

103. Mysore, M. R., Margraf, L. R., Jaramillo, M. A., Breed, D. R., Chau, V. L., Arevalo, M. & Moya, F. R. Surfactant protein A is decreased in a rat model of congenital diaphragmatic hernia. *Am. J. Respir. Crit. Care Med.* **157**, 654-657 (1998).

104. Losada, A., Xia, H., Migliazza, L., Diez-Pardo, J. A., Santisteban, P. & Tovar, J. A. Lung hypoplasia caused by nitrofen is mediated by down-regulation of thyroid transcription factor TTF-1. *Pediatr. Surg. Int.* **15**, 188-191 (1999).

105. Sullivan, K. M., Hawgood, S., Flake, A. W., Harrison, M. R. & Adzick, N. S. Amniotic fluid phospholipid analysis in the fetus with congenital diaphragmatic hernia. *J. Pediatr. Surg.* **29**, 1020-3; discussion 1023-4 (1994).

106. IJsselstijn, H., Zimmermann, L. J., Bunt, J. E., de Jongste, J. C. & Tibboel, D. Prospective evaluation of surfactant composition in bronchoalveolar lavage fluid of infants with congenital diaphragmatic hernia and of age-matched controls. *Crit. Care Med.* **26**, 573-580 (1998).

107. Cogo, P. E., Zimmermann, L. J., Rosso, F., Tormena, F., Gamba, P., Verlato, G., Baritussio, A. & Carnielli, V. P. Surfactant synthesis and kinetics in infants with congenital diaphragmatic hernia. *Am. J. Respir. Crit. Care Med.* **166**, 154-158 (2002).

108. Boucherat, O., Benachi, A., Chailley-Heu, B., Franco-Montoya, M. L., Elie, C., Martinovic, J. & Bourbon, J. R. Surfactant maturation is not delayed in human fetuses with diaphragmatic hernia. *PLoS Med.* **4**, e237 (2007).

109. Van Meurs, K. & Congenital Diaphragmatic Hernia Study Group. Is surfactant therapy beneficial in the treatment of the term newborn infant with congenital diaphragmatic hernia? *J. Pediatr.* **145**, 312-316 (2004).

110. Lally, K. P., Lally, P. A., Langham, M. R., Hirschl, R., Moya, F. R., Tibboel, D., Van Meurs, K. & Congenital Diaphragmatic Hernia Study Group. Surfactant does not improve survival rate in preterm infants with congenital diaphragmatic hernia. *J. Pediatr. Surg.* **39**, 829-833 (2004).

111. Chen, H., Zhuang, F., Liu, Y. H., Xu, B., Del Moral, P., Deng, W., Chai, Y., Kolb, M., Gauldie, J., Warburton, D., Moses, H. L. & Shi, W. TGF-beta receptor II in epithelia versus mesenchyme plays distinct roles in the developing lung. *Eur. Respir. J.* **32**, 285-295 (2008).

112. Shi, W., Xu, J. & Warburton, D. Development, repair and fibrosis: what is common and why it matters. *Respirology* **14**, 656-665 (2009).

113. De Langhe, S. P., Sala, F. G., Del Moral, P. M., Fairbanks, T. J., Yamada, K. M., Warburton, D., Burns, R. C. & Bellusci, S. Dickkopf-1 (DKK1) reveals that fibronectin is a major target of Wnt signaling in branching morphogenesis of the mouse embryonic lung. *Dev. Biol.* **277**, 316-331 (2005).

114. Sakai, T., Larsen, M. & Yamada, K. M. Fibronectin requirement in branching morphogenesis. *Nature* **423**, 876-881 (2003).

115. Lemmens, K., Doggen, K. & De Keulenaer, G. W. Role of neuregulin-1/ErbB signaling in cardiovascular physiology and disease: implications for therapy of heart failure. *Circulation* **116**, 954-960 (2007).

116. Dammann, C. E., Nielsen, H. C. & Carraway, K. L.,3rd. Role of neuregulin-1 beta in the developing lung. *Am. J. Respir. Crit. Care Med.* **167**, 1711-1716 (2003).

117. Gregory, P. A., Bracken, C. P., Smith, E., Bert, A. G., Wright, J. A., Roslan, S., Morris, M., Wyatt, L., Farshid, G., Lim, Y. Y., Lindeman, G. J., Shannon, M. F., Drew, P. A., Khew-Goodall, Y. & Goodall, G. J. An autocrine TGF-beta/ZEB/miR-200 signaling network regulates establishment and maintenance of epithelial-mesenchymal transition. *Mol. Biol. Cell* **22**, 1686-1698 (2011).

118. Wojdacz, T. K., Dobrovic, A. & Hansen, L. L. Methylation-sensitive high-resolution melting. *Nat. Protoc.* **3**, 1903-1908 (2008).